bioRxiv preprint doi: https://doi.org/10.1101/824995; this version posted May 25, 2020. The copyright holder for this preprint (which was not certified by peer review) is the author/funder, who has granted bioRxiv a license to display the preprint in perpetuity. It is made available under aCC-BY 4.0 International license.

Dectin-1 Molecular Aggregation and Signaling is Sensitive to β-Glucan Structure and Glucan Exposure on *Candida albicans* Cell Walls

Authors:

Eduardo U. Anaya[1], Akram Etemadi Amin[1,2], Michael J. Wester[3], Michael E. Danielson[4], Kyle S. Michel[4], Aaron K. Neumann[1,5]

Affiliations:

1. Department of Pathology, University of New Mexico, School of Medicine, Albuquerque, NM, USA, 87131

2. Department of Physics and Astronomy, University of New Mexico, Albuquerque, NM, USA 87131

3. Department of Mathematics and Statistics, University of New Mexico, Albuquerque, NM, USA, 87131

4. ImmunoResearch Inc., Eagan, MN, USA, 55121

5. Corresponding author: akneumann@salud.unm.edu

Keywords:

Dectin-1, dimer, β-Glucan, *Candida albicans*, hemITAM, Syk, Calcium signaling, (Förster Resonance Energy Transfer) FRET, Raster Image Correlation Spectroscopy (RICS), Numbers & Brightness analysis (N&B)

bioRxiv preprint doi: https://doi.org/10.1101/824995; this version posted May 25, 2020. The copyright holder for this preprint (which was not certified by peer review) is the author/funder, who has granted bioRxiv a license to display the preprint in perpetuity. It is made available under aCC-BY 4.0 International license.

Abstract

Dectin-1A is a C-type Lectin innate immunoreceptor that recognizes β-(1,3;1,6)-glucan, a structural component of *Candida* species cell walls. The higher order structure of β-glucans ranges from random coil to insoluble fiber due to varying degrees of tertiary (helical) and quaternary structure. Model *Saccharomyces cerevisiae* β-glucans of medium and high molecular weight (MMW and HMW, respectively) are highly structured. In contrast, low MW glucan (LMW) is much less structured. Despite similar affinity for Dectin-1A, the ability of glucans to induce Dectin-1A mediated calcium influx and Syk phosphorylation positively correlates with their degree of higher order structure. Chemical denaturation and renaturation of MMW glucan showed that glucan structure determines agonistic potential, but not binding affinity, for Dectin-1A. We explored the role of glucan structure on Dectin-1A oligomerization, which is thought to be required for Dectin-1 signaling. Glucan signaling decreased Dectin-1A diffusion coefficient in inverse proportion to glucan structural content, which was consistent with Dectin-1A aggregation. Förster Resonance Energy Transfer (FRET) measurements revealed that molecular aggregation of Dectin-1 occurs in a manner dependent upon glucan higher order structure. Number and Brightness analysis specifically confirmed an increase in the Dectin-1A dimer and oligomer populations that is correlated with glucan structure content. Comparison of receptor modeling data with FRET measurements confirms that in resting cells, Dectin-1A is predominantly in a monomeric state. Super Resolution Microscopy revealed that glucan-stimulated Dectin-1 aggregates are very small (<15 nm) collections of a few engaged receptors. Finally, FRET measurements confirmed increased molecular aggregation of Dectin-1A at fungal particle contact sites in a

bioRxiv preprint doi: https://doi.org/10.1101/824995; this version posted May 25, 2020. The copyright holder for this preprint (which was not certified by peer review) is the author/funder, who has granted bioRxiv a license to display the preprint in perpetuity. It is made available under aCC-BY 4.0 International license.

45 manner that positively correlated with the degree of exposed glucan on the particle
46 surface. These results indicate that Dectin-1A senses the solution conformation of β-
47 glucans through their varying ability to drive receptor dimer/oligomer formation and
48 activation of membrane proximal signaling events.
49

50 **Introduction**

51 Overall, *Candida* infections have increased over the past 20 years in the United States
52 [1–5]. It is estimated that 46,000 cases of healthcare-associated invasive candidiasis
53 occur in the United States annually [6]. The fungal cell wall is composed of an inner
54 layer of chitin, a middle layer of β(1,3;1,6)-D-glucan and an outer layer of N- and O-
55 linked mannans [7]. During infection, the cell wall of *Candida* is an important and
56 relevant virulence factor, playing roles in adhesion, colonization and immune recognition
57 [8,9].
58 Due to the abundant amount of mannan in the outer cell wall, β-glucan exhibits a very
59 limited, punctate pattern of nanoscale surface exposure. The extent of this glucan
60 masking is influenced by environmental conditions such as intestinal pH or lactate levels
61 [10,11]. In addition, interactions with neutrophils have been shown to “unmask” the
62 mannose layer through a neutrophil extracellular trap-mediated mechanism [12].
63 Furthermore, our lab and others have determined that anti-fungal drugs “unmask” the
64 fungal cell wall, which leads to increases in nanoscale regions of glucan exposure and
65 correlates with enhanced host defense [13–15]. Therefore, fungal species use masking
66 as a way to evade immune recognition of β-glucan by the host’s immune system [16].

bioRxiv preprint doi: https://doi.org/10.1101/824995; this version posted May 25, 2020. The copyright holder for this preprint (which was not certified by peer review) is the author/funder, who has granted bioRxiv a license to display the preprint in perpetuity. It is made available under aCC-BY 4.0 International license.

β-glucans consist of a β-1,3-linked backbone with side chains of β-1,6-linked units that vary in length and degree of branching [17]. β-glucan forms triple-helical structures through intermolecular hydrogen bonds with two other strands [17–21]. This triple helix conformation is shown to form with just the β-1,3-linked backbone, however β-1,6-linked side chains play an important role in determination of the triple helix cavity formation through side chain/side chain interactions [21].

β-glucans are known for their biological activities such as enhancing anti-tumor, anti-bacterial, and anti-viral immunity as well as wound healing [22–25]. The biological activity of glucan is affected by its structure, size, structural modification, conformation and solubility [26]. Research has found that branching is not required to observe biological activity, but branching has been shown to enhance binding to the Dectin-1 receptor [27]. In contrast, β-glucan size is thought to play a major role in biological activity with glucans that are shorter than 10,000 Da being generally inactive *in vivo* [28,29]. However, despite having similar sizes, glucans can display differences in their biological activities [30–32]. For example, studies have demonstrated that the immunoregulatory activity of variously sourced laminarin ranges from agonistic to antagonistic depending on its physicochemical properties, purity and structure [33]. Furthermore, β-glucans that have a triple helical conformation are more potent agonists of host immune response than single helical glucan [27,34–36]. We propose that the β-glucan triple-helix conformation plays an important role in determining the biological activity of the β-glucan through modulating the degree of receptor oligomerization upon ligation.

bioRxiv preprint doi: https://doi.org/10.1101/824995; this version posted May 25, 2020. The copyright holder for this preprint (which was not certified by peer review) is the author/funder, who has granted bioRxiv a license to display the preprint in perpetuity. It is made available under aCC-BY 4.0 International license.

89 During innate immune recognition of *Candida*, the organization of cell wall ligands and
90 pattern recognition receptors is an important determinant of successful immune
91 activation [8]. The fungi-responsive C-type lectin (CTL) anti-fungal immunoreceptors
92 play a central role in the detection of *Candida* [37]. Human Dectin-1A is the main CTL
93 that recognizes the β-glucan found in the fungal cell wall [38–40]. Dectin-1A is found in
94 myeloid lineage cells, and once activated, it stimulates phagocytic activity, the
95 production of reactive oxygen intermediates and inflammatory mediators. Dectin-1A
96 contains a CTL-like domain, separated from the cell membrane by a glycosylated stalk
97 region, a transmembrane domain and an intracellular cytosolic domain. Dectin-1
98 contains half an Immunoreceptor Tyrosine-based Activation Motif (a YXXL sequence
99 with an upstream stretch of acidic amino acids) in its cytoplasmic tail, which is termed a
100 (hem)ITAM domain [41,42]. Monophosphorylated ITAM domains, which are anticipated
101 to approximate the structure of phosphorylated (hem)ITAM domains, poorly recruit and
102 activate Syk for downstream signaling because they cannot support bivalent
103 engagement of both of Syk's SH2 domains [43]. Another (hem)ITAM bearing receptor,
104 CLEC-2, is reported to require dimerization for its signaling [44]. By analogy to this and
105 other (hem)ITAM receptors, it is speculated that Dectin-1A must oligomerize to
106 recapitulate a multivalent binding site for Syk to facilitate signal transduction [8,44,45].
107 However, this prediction has not been directly explored for Dectin-1A in live cells at the
108 molecular level with relation to signaling outcomes.
109 In this study, we propose that factors that induce an aggregated membrane organization
110 of Dectin-1A during activation are very important for determining signaling outcomes of
111 Dectin-1A engagement by β-glucan [44,45]. We hypothesize that ligand structure, at the

bioRxiv preprint doi: https://doi.org/10.1101/824995; this version posted May 25, 2020. The copyright holder for this preprint (which was not certified by peer review) is the author/funder, who has granted bioRxiv a license to display the preprint in perpetuity. It is made available under aCC-BY 4.0 International license.

112 levels of glucan tertiary and quaternary structure as well as nanoscale glucan
113 exposures on the pathogen surface, impacts signaling by determining the membrane
114 organization and spatiotemporal clustering dynamics of Dectin-1A. To test this
115 hypothesis, we stimulated HEK-293 cells transfected with Dectin-1A with a variety of
116 soluble β-glucans that have different structures and sizes. We chose to work in this
117 model system because it provides a simplified platform necessary to investigate the
118 physical biology of Dectin-1A activation by isolating Dectin-1A signaling from the
119 complex milieu of other receptors and other Dectin-1 isoforms expressed in innate
120 immunocytes. Also, this model facilitates the expression of multiple fluorescent protein-
121 tagged Dectin-1A constructs necessary to the work. Using calcium imaging and western
122 blotting assays, our results revealed that Dectin-1A activation is influenced by the β-
123 glucan triple helical structure. Furthermore, our subcellular FRET measurements by
124 Fluorescence Lifetime Imaging Microscopy (FLIM-FRET), as well as application of
125 fluorescence correlation spectroscopy approaches, revealed dimerization and
126 oligomerization of Dectin-1A when stimulated with highly structured β-glucans. In
127 addition, these dimerization events occurred in fungal contact sites of fungal cells with
128 high glucan exposure. Together, our findings indicate β-glucan structure is required for
129 Dectin-1A to form dimeric and oligomeric membrane aggregates.
130

131 **Results**

132 **Dectin-1A activation is dependent on the molecular weight of the soluble β-**
133 **glucan.**

bioRxiv preprint doi: https://doi.org/10.1101/824995; this version posted May 25, 2020. The copyright holder for this preprint (which was not certified by peer review) is the author/funder, who has granted bioRxiv a license to display the preprint in perpetuity. It is made available under aCC-BY 4.0 International license.

β-glucans, existing as insoluble fibers in the cell wall, are likely to have a high degree of tertiary and quaternary structure. So, an encounter with highly structured glucan might be indicative of a pathogen cell wall structure. Furthermore, less structured glucans are encountered by Dectin-1A physiologically [41]. Small soluble circulating glucan can derive from sloughed cell wall material or from dietary absorption [46–49]. However, there is not much known about Dectin-1A's ability to distinguish between highly structured β-glucan found on cell walls of fungal pathogens and less structured glucans found in circulation. Therefore, we examined how Dectin-1A activation is affected by glucans with different quaternary and tertiary structures. To accomplish this, we used high molecular weight (HMW 450 kDa), medium molecular weight (MMW 145 kDa), and low molecular weight (LMW 11 kDa) soluble glucans, in decreasing order of tertiary and quaternary structures, derived from *S. cerevisiae* cell walls. These *S. cerevisiae* glucans in soluble form or as particulate "zymosan" are common models for stimulation of innate immunocytes by fungal pathogen cell wall glucan. The above glucans have overall very similar composition and structures to *C. albicans* yeast glucan, though relatively minor differences in β-(1,6)-glucan side chain length and branching frequency have been reported between these species [50,51].

Using these glucans, we performed intracellular calcium ($[Ca^{2+}]_i$) measurement experiments on HEK-293 cells (lacking endogenous Dectin-1 expression) transfected with Dectin-1A. We stimulated the cells using either LMW, MMW, or HMW glucan. All the glucans induced a significant increase in peak amplitude $[Ca^{2+}]_i$ compared to unstimulated cells (Fig.1 A,B). We found that large, highly ordered glucans (HMW and MMW) induced a significant, Dectin-1 dependent increase in peak amplitude of $[Ca^{2+}]_i$

bioRxiv preprint doi: https://doi.org/10.1101/824995; this version posted May 25, 2020. The copyright holder for this preprint (which was not certified by peer review) is the author/funder, who has granted bioRxiv a license to display the preprint in perpetuity. It is made available under aCC-BY 4.0 International license.

compared to LMW, with MMW having the highest peak amplitude (Fig. 1C). Interestingly, the response to MMW glucan was uniform at the single cell level. However, cells stimulated with HMW glucan exhibited a more heterogeneous response, with some cells achieving comparable maximum amplitudes as with MMW and others exhibiting little change from basal calcium levels (Fig. 1A, B). We expect that HMW glucan is present as larger particles than MMW, so at equal mass/volume concentrations, the HMW solution will have a lower concentration of particles. Non-responder cells in HMW experiments may have stochastically encountered too few glucan particles to achieve a detectable signaling response. When we stimulated cells with MMW or HMW at equimolar concentrations, which should have similar glucan particulate concentrations, we observed a minor difference in peak amplitude, but we saw that the integrated Ca^{2+} flux over time was the same for MMW and HMW glucans (Supplemental Fig. 1). Furthermore, single cell data demonstrated a similarly uniform response of Dectin-1 to MMW and HMW glucans under these conditions. These results indicate that Dectin-1A drives differential Ca^{2+} flux to glucan ligands that vary in size and structure.

To determine how these differently-structured, soluble glucans impacted cellular patterns of Syk phosphorylation, we stimulated HEK-293 cells expressing Dectin1A-mEmerald with H_2O (vehicle), LMW, MMW, or HMW. Whole cell lysate was collected and Syk phosphorylation was determined by western blot analysis. Likewise, our results show an increase in Syk phosphorylation in the larger, highly structured glucan MMW and HMW compared to unstimulated and LMW stimulated cells (Fig. 1 D,E). Additionally, Syk inhibitors abrogated calcium signaling of Dectin-1A when stimulated

bioRxiv preprint doi: https://doi.org/10.1101/824995; this version posted May 25, 2020. The copyright holder for this preprint (which was not certified by peer review) is the author/funder, who has granted bioRxiv a license to display the preprint in perpetuity. It is made available under aCC-BY 4.0 International license.

with MMW glucan (Fig. 1F). These results indicate that glucans with higher order structure are better able to activate Dectin-1A-mediated Ca^{2+} signaling and that this is a Syk dependent process.

bioRxiv preprint doi: https://doi.org/10.1101/824995; this version posted May 25, 2020. The copyright holder for this preprint (which was not certified by peer review) is the author/funder, who has granted bioRxiv a license to display the preprint in perpetuity. It is made available under aCC-BY 4.0 International license.

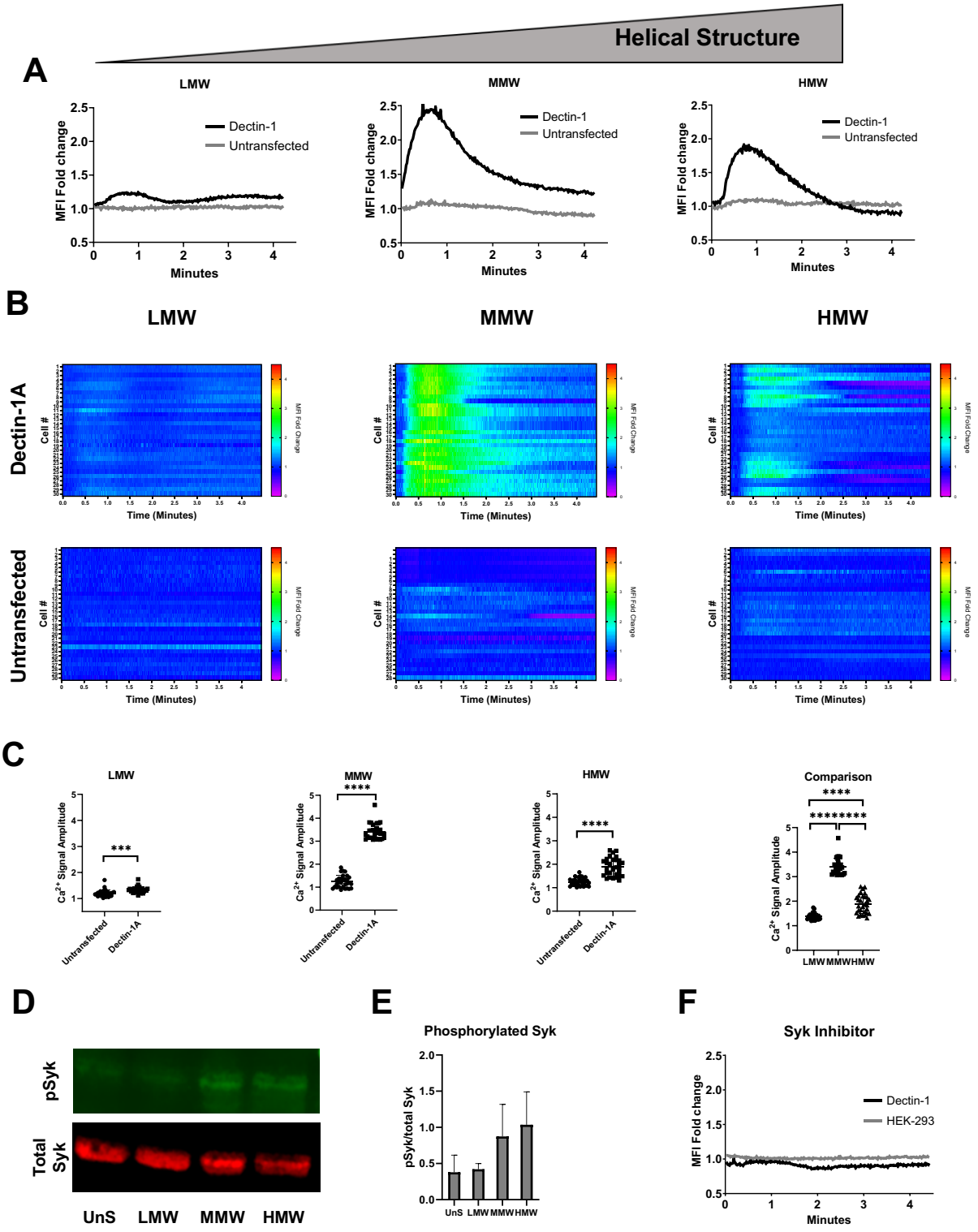

Figure 1. Differential signaling response of Dectin-1A to soluble β-glucan.

bioRxiv preprint doi: https://doi.org/10.1101/824995; this version posted May 25, 2020. The copyright holder for this preprint (which was not certified by peer review) is the author/funder, who has granted bioRxiv a license to display the preprint in perpetuity. It is made available under aCC-BY 4.0 International license.

(A) HEK-293 cells stably transfected with Dectin-1A were loaded with Fluo-4 and Cell Tracker Deep Red at equimolar concentrations. Cell Tracker Deep Red was simultaneously loaded in order to normalize for changes in cytosolic volume caused from cell contraction. The mean fluorescence intensity of 30 cells was averaged for Dectin-1A transfected (black) or untransfected (grey) HEK-293 cells stimulated with LMW, MMW, or HMW glucan at 1 μg/ml. (n = 30 per glucan from 3 independent experiments per glucan). Data shown as mean fold change in volume-normalized $[Ca^{2+}]_{intracellular}$. (B) Heat maps of relative changes in intracellular calcium concentration of untransfected or Dectin-1A transfected individual cells upon addition of either LMW, MMW, or HMW glucan. Each row represents the normalized ratio of Fluo-4 and Cell Tracker Deep Red for a single cell over time. (C) Maximum signal amplitude of single cells treated with LMW, MMW, or HMW glucan showing Dectin-1 dependent glucan responses. Statistical comparison of maximum amplitudes for Dectin-1 expressing cells treated with each of the three glucans is shown in the far right panel. Data shown as mean ± SD (n = 30 per glucan from 3 independent experiments per glucan). One-way ANOVA with multiple comparisons by the Dunnett test, *** $p<0.0001$, **** $p<0.000001$. (D) Cell lysates were collected at 5 min after stimulation and analyzed by Western blotting using antibodies against p-Syk and Syk. The intensity of p-Syk was normalized against total Syk. (E) Quantification of the western blot normalized p-Syk/Syk signal is shown as mean ± SD of n = 3 independent experimental replicates. (F) Untransfected (grey) and stably transfected Dectin-1A (black) HEK-293 cells were loaded with Fluo-4 and Cell Tracker Deep Red at equimolar concentrations and treated with Syk Inhibitor at 250 nM, then stimulated with MMW glucan. Average mean fluorescence intensity of 30 cells was observed for cells stimulated with MMW glucan at 1 μg/ml. (n = 30 from 3 independent experiments).

β-glucan denaturation abrogates its potential for Dectin-1A activation

To determine if the glucan structure affects signaling outcomes, we denatured MMW (highly stimulatory glucan) using DMSO, a chaotrope that promotes a reduction in glucan tertiary structure, thus shifting MMW's triple helix structure to a more single helical or random coil structure [17]. The results showed that when we denatured MMW

bioRxiv preprint doi: https://doi.org/10.1101/824995; this version posted May 25, 2020. The copyright holder for this preprint (which was not certified by peer review) is the author/funder, who has granted bioRxiv a license to display the preprint in perpetuity. It is made available under aCC-BY 4.0 International license.

glucan, we did not observe calcium signaling in cells expressing Dectin-1A (Fig. 2A, B). However, when we renatured the glucans by removing DMSO via dialysis we observe partial recovery of calcium signaling. We found that renatured glucans induce a significant increase in peak amplitude $[Ca^{2+}]_i$ response compared to DMSO denatured MMW and renatured MMW stimulated untransfected HEK-293 cells (Fig. 2 C). In addition, we confirmed the loss of helical structure via a Congo Red assay. Congo Red specifically binds to β-(1,3)-glucans with a triple helix conformation as their tertiary structure. This binding is detected by bathochromic shift in absorbance maximum from 488 to 516 nm [52]. Our results indicated a loss in glucan structure after denaturation in a DMSO solution that was regained upon renaturation (Fig. 2 D). Moreover, we repeated these experiments by stimulating cells with glucan denatured with NaOH or neutralized renatured glucan [17]. Similarly, our results show that cells lose the ability to activate Dectin-1A calcium signaling when stimulated with denatured MMW glucan but regain the ability to stimulate Dectin-1A activation when the glucan is renatured (Fig. 2 E,F). We found that renatured glucans induce a significant increase in peak amplitude $[Ca^{2+}]_i$ response compared to NaOH denatured MMW and renatured MMW stimulated untransfected HEK-293 cells (Fig. 2 G). In addition, we confirmed that glucan structure was lost when NaOH was added and regained when neutralized (Fig. 2 H). These results suggest that glucan structure is an important factor in activating a Dectin-1A response.

bioRxiv preprint doi: https://doi.org/10.1101/824995; this version posted May 25, 2020. The copyright holder for this preprint (which was not certified by peer review) is the author/funder, who has granted bioRxiv a license to display the preprint in perpetuity. It is made available under aCC-BY 4.0 International license.

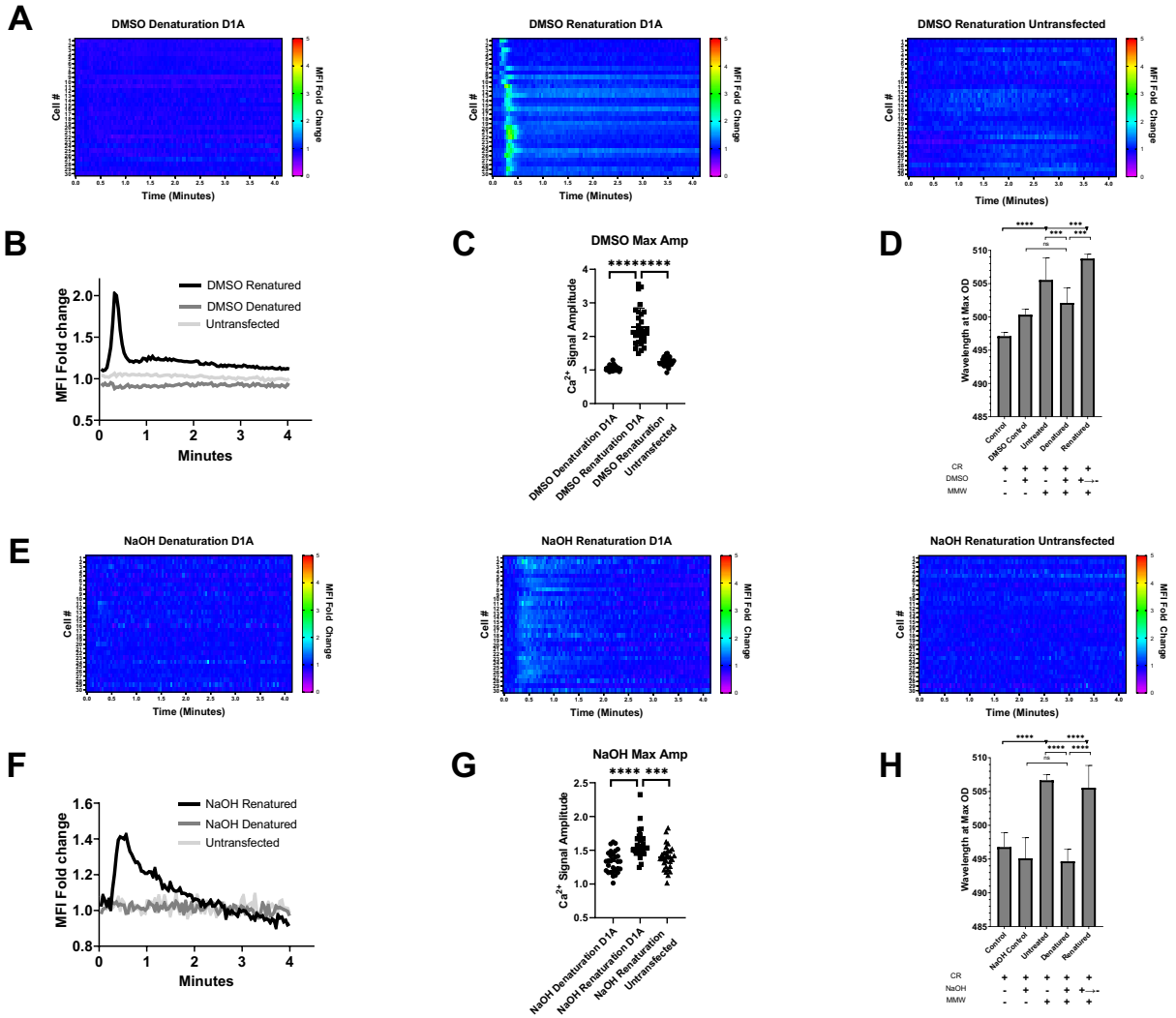

232

233 **Figure 2: Glucan higher order structure is a critical determinant of its stimulatory**

234 **potential.**

235 (A) HEK-293 cells stably expressing Dectin-1A or untransfected were loaded with Fluo-4 and Cell Tracker

236 Deep Red at equimolar concentrations. Heat maps show relative changes in intracellular calcium

237 concentration of untransfected or Dectin-1A transfected individual cells upon either addition of DMSO

238 denatured MMW glucan or renatured MMW glucan. Each row represents the normalized ratio of Fluo-4

239 and Cell Tracker Deep Red for a single cell over time. (B) Average mean fluorescence intensity of 30 cells

240 stimulated with DMSO denatured/renatured MMW glucan was observed. (n = 30 from 3 independent

241 experiments). (C) Maximum amplitude of single cells treated with DMSO denatured or renatured MMW

bioRxiv preprint doi: https://doi.org/10.1101/824995; this version posted May 25, 2020. The copyright holder for this preprint (which was not certified by peer review) is the author/funder, who has granted bioRxiv a license to display the preprint in perpetuity. It is made available under aCC-BY 4.0 International license.

glucan. Data shown as mean ± SD (n = 30 from 3 independent experiments). One-way ANOVA with multiple comparisons by the Dunnett test, **** p<0.000001. (D) 1 mg/ml of MMW glucan was denatured using DMSO and incubated with Congo Red. Control samples contained Congo Red and DMSO. Renaturation was accomplished by dialyzing out DMSO 24 hrs prior to the experiment. Data shown as mean ± SD (n = 9 from 3 independent experiments). (E) HEK-293 cells stably expressing Dectin-1A or untransfected were loaded with Fluo-4 and Cell Tracker Deep Red at equimolar concentrations. Heat maps show relative changes in intracellular calcium concentration of untransfected or Dectin-1A transfected cells upon either addition of NaOH denatured or renatured MMW glucan. Each row represents the normalized ratio of Fluo-4 and Cell Tracker Deep Red for a single cell over time. (F) Average mean fluorescence intensity of 30 cells stimulated with NaOH denatured/renatured MMW glucan was observed. (n = 30 from 3 independent experiments). (G) Maximum amplitude of single cells treated with NaOH denatured or renatured MMW glucan. Data shown as mean ± SD (n = 30 from 3 independent experiments). One-way ANOVA with multiple comparisons by the Dunnett test, **** p<0.000001. (H) 1 mg/ml of MMW glucan was denatured using NaOH and incubated with Congo Red. Control samples contained NaOH and Congo Red. Renaturation was accomplished by neutralizing NaOH. Data shown as mean ± SD (n = 9 from 3 independent experiments). Welch's t-test, ** p<0.001, *** p<0.0001, **** p<0.000001.

β-glucan structure variation and manipulation does not alter affinity for Dectin-1

We considered the possibility that these soluble glucans might have different affinities for Dectin-1A, resulting in differential receptor activation. Thus, we conducted biolayer interferometry experiments to determine the binding affinity of these glucans to the carbohydrate recognition domain of Dectin-1A. This was accomplished using a chimeric fusion protein of the carbohydrate recognition domain of Dectin-1A and the human IgG Fc region. An anti-human IgG Fc Capture biosensor tip was used to load this fusion protein. Association and dissociation curves of the glucan and fusion protein where then

bioRxiv preprint doi: https://doi.org/10.1101/824995; this version posted May 25, 2020. The copyright holder for this preprint (which was not certified by peer review) is the author/funder, who has granted bioRxiv a license to display the preprint in perpetuity. It is made available under aCC-BY 4.0 International license.

collected. The results shown in Fig. 3A indicate that all the glucans have approximately nanomolar dissociation constants for Dectin-1A carbohydrate recognition domain despite the previously described differences in signaling [27]. Weight average molecular weights of purified *Saccharomyces cerevisiae* β -(1,3)-glucan fractions vary over an approximate 40-fold range, but there is relatively little difference between these glucans' apparent affinity for the Dectin-1 carbohydrate recognition domain.

Furthermore, to determine differences in the structure of these glucans, we analyzed the conformational transition of triple helix to random coil of β-1,3-D-glucans through denaturation experiments. Experiments were conducted by denaturing glucans with NaOH at various concentrations in the presence of Congo Red. Our results show that the amount of glucan tertiary structure scales with molecular weight as measured by the concentration of NaOH required to reduce Congo Red binding to glucan (Fig. 3B), suggesting that the size of the glucans is correlated with their higher-order structure. Together, these results indicate that downstream signaling of the receptor is determined by the structure of the glucan rather than affinity alone.

bioRxiv preprint doi: https://doi.org/10.1101/824995; this version posted May 25, 2020. The copyright holder for this preprint (which was not certified by peer review) is the author/funder, who has granted bioRxiv a license to display the preprint in perpetuity. It is made available under aCC-BY 4.0 International license.

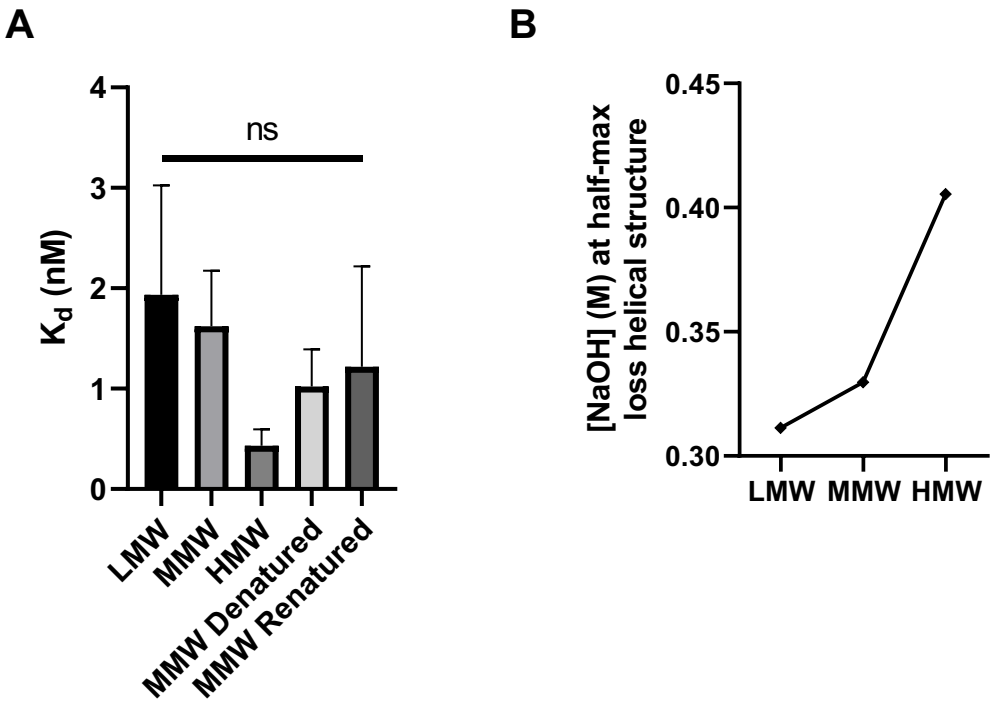

Figure 3: Characterization of Dectin-1 binding affinity and helical structure of fungal cell wall glucans used in this study.

(A) Biolayer interferometry experiments were conducted on LMW, MMW, HMW, MMW denatured, and MMW renatured glucans using an anti-human IgG Fc Capture biosensor tip and a Dectin-1A-Fc fusion protein. Data shown as mean ± SD (n = 3 from 3 independent experiments). Statistical comparison by one-way ANOVA. (B) LMW, MMW, and HMW β-glucans were denatured using 0M-1M NaOH in the presence of Congo Red. Concentration of NaOH at which absorbance (516 nm) decreased to the half-maximal value was plotted. Data shown as mean ± SD (n = 9 from 3 independent experiments).

Dectin-1A decreases in diffusion coefficient when stimulated with highly structured β-glucans

The Stokes-Einstein equation predicts that if a diffusing object increases in hydrodynamic radius, it will slow down proportionally to that change. We measured the diffusion coefficient of Dectin-1A pre/post glucan stimulation to determine whether the

bioRxiv preprint doi: https://doi.org/10.1101/824995; this version posted May 25, 2020. The copyright holder for this preprint (which was not certified by peer review) is the author/funder, who has granted bioRxiv a license to display the preprint in perpetuity. It is made available under aCC-BY 4.0 International license.

298 receptor diffusion coefficient decreased, potentially due to increasing hydrodynamic
299 radius as an initially monomeric receptor formed larger clusters/oligomers. We obtained
300 average diffusion coefficients and spatial number density of our receptor using Raster
301 Image Correlation Spectroscopy (RICS). RICS allowed us to survey multiple areas of
302 the cell for molecular parameters such as diffusion coefficient and receptor density.
303 This section pertains to receptor diffusion measurement by RICS, while receptor density
304 is treated in a separate section below. Furthermore, because fluorescence was probed
305 within a large cell area, RICS analyses suffered much less from photobleaching and
306 location specific artifacts than analogous single-point measurements. Previous research
307 has described RICS in more detail [53,54]. Briefly, we generated a volume of excitation
308 using focused laser illumination and calibrated a confocal observation volume using
309 standard fluorophores of known diffusion coefficient. We observed fluorescent
310 molecules (i.e., Dectin-1A-mEmerald) diffusing in and out of this excitation volume
311 through fluctuation in the number of photons obtained. Experimentally observed
312 fluorescence correlations at various spatiotemporal lags were then fit to a 2D
313 autocorrelation function to obtain the receptor diffusion coefficient in the observed
314 membrane (Fig. 4A).
315 Using HEK-293 cells expressing Dectin-1A-mEmerald, we conducted RICS
316 measurements before and after stimulation with soluble β-glucans. We determined that
317 cells stimulated with MMW or HMW exhibited a significant decrease in mobility
318 compared to LMW and unstimulated cells (Fig. 4B). This finding is consistent with an
319 increase in receptor aggregation upon stimulation, which we examine in greater detail
320 below. We proceeded to conduct additional membrane biophysical studies to further

bioRxiv preprint doi: https://doi.org/10.1101/824995; this version posted May 25, 2020. The copyright holder for this preprint (which was not certified by peer review) is the author/funder, who has granted bioRxiv a license to display the preprint in perpetuity. It is made available under aCC-BY 4.0 International license.

test for changes in the molecular aggregation state of Dectin-1 during stimulation with glucan.

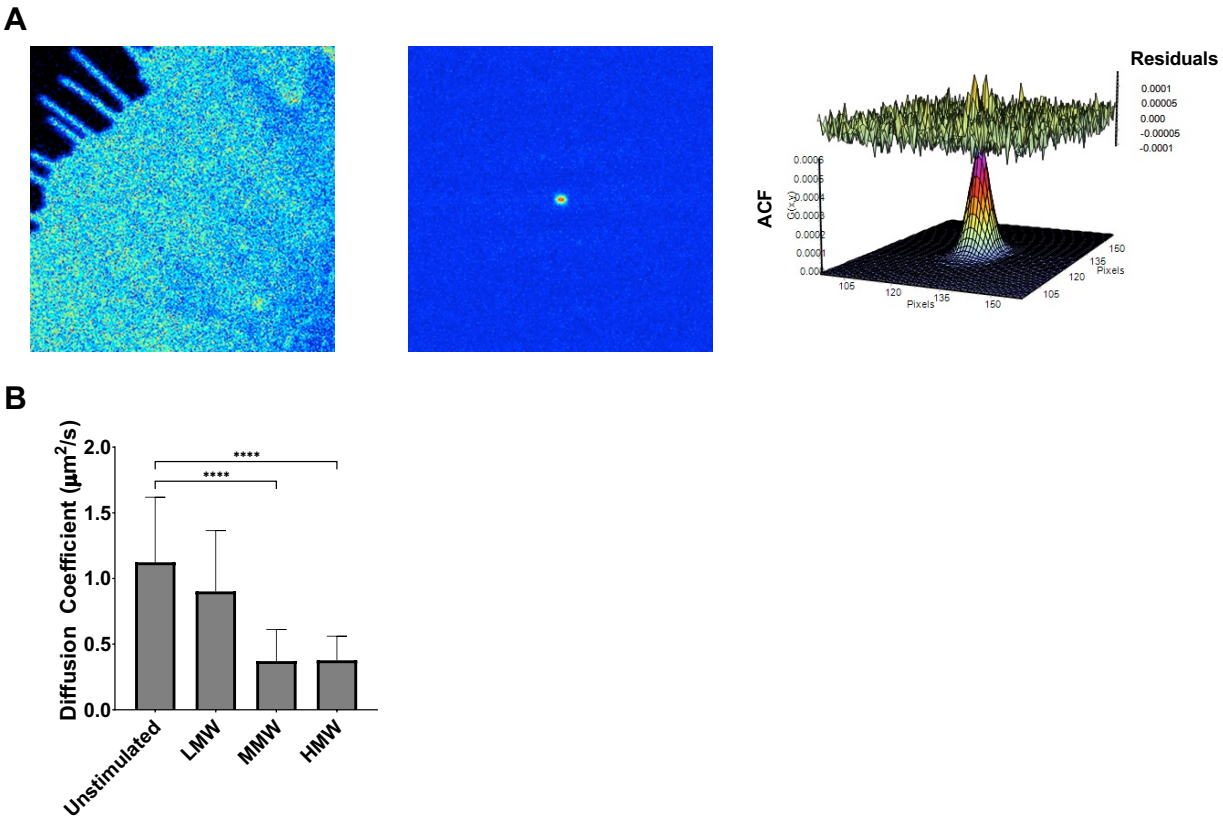

Figure 4: Dectin-1A surface diffusion coefficient decreases when stimulated with highly structured β-glucans.

(A) A representative example of Raster Image Correlation Spectroscopy (RICS) analysis. (Left) Representative RICS image of HEK-293 cells expressing Dectin-1A-mEmerald. (Middle) Autocorrelation function (ACF) calculated from the time series. Red represents a high ACF value, blue represents a low ACF value. (Right) Fit of the ACF to a Gaussian diffusion model to calculate the diffusion coefficient. (B) RICS analysis of fluorescently tagged Dectin-1A expressed in HEK-293 provided average diffusion coefficient for cells that were unstimulated or stimulated with LMW, MMW, or HMW. Data shown as mean ± SD (n = 30); One-Way ANOVA multiple comparison test, **** $p<0.00001$.

bioRxiv preprint doi: https://doi.org/10.1101/824995; this version posted May 25, 2020. The copyright holder for this preprint (which was not certified by peer review) is the author/funder, who has granted bioRxiv a license to display the preprint in perpetuity. It is made available under aCC-BY 4.0 International license.

Dectin-1A forms dimers/oligomers when stimulated with highly structured β-glucans

The results shown above indicate that the β-glucan structure is an important factor in signaling outcomes. Previous research has shown that other transmembrane CTLs that also contain a (hem)ITAM domain can form homodimers before or upon ligand recognition [55,56]. Furthermore, crystallography studies of the carbohydrate recognition domain (CRD) have shown that Dectin-1A head groups form dimers when laminaritriose is present [57]. Additionally, size exclusion chromatography with multi-angle light scattering analysis has described Dectin-1 ligand-induced tetramer (or dimer-of-dimers) formation in solution [57,58]. In line with these ideas, we sought to examine how ligand structure impacts signaling by determining the dimerization/oligomerization of full length Dectin-1A in living cell membranes.

To assess changing molecular proximity of Dectin-1 proteins, we employed Fluorescence Lifetime Imaging Microscopy for Forster Resonance Energy Transfer (FLIM-FRET). FRET based imaging capitalizes on close proximity of two proteins to visualize protein-protein interactions, including receptor dimerization and receptor-ligand complex formation [59]. FLIM characterizes the duration of a fluorophore's excited state before returning to the ground state. The occurrence of FRET causes rapid quenching of donor fluorescence, so FRET can be determined by measuring the shortening of donor fluorescence lifetime when in proximity to acceptor. FLIM-FRET offers the opportunity of studying *in vivo* receptor interactions in a direct, spatially resolved manner. We examined Dectin-1A engagement using FLIM-FRET on HEK-293 cells co-expressing two fluorescent Dectin-1 constructs—N-terminally tagged Dectin-1A-

bioRxiv preprint doi: https://doi.org/10.1101/824995; this version posted May 25, 2020. The copyright holder for this preprint (which was not certified by peer review) is the author/funder, who has granted bioRxiv a license to display the preprint in perpetuity. It is made available under aCC-BY 4.0 International license.

357 mEmerald (donor) and Dectin-1A-mCherry (acceptor)—both having their fluorophores
358 on the cytoplasmic face of the plasma membrane, and then stimulated the cells with
359 soluble β-glucan. Analysis was conducted on the plasma membrane itself by masking
360 out internal cellular compartments (Fig. 5A). FRET efficiency is a parameter that
361 exhibits an inverse 6th power dependence upon donor-acceptor distance. Donor-
362 acceptor percentage is simply the percentage of all donors that are involved in FRET
363 interactions at a given time. These parameters were determined experimentally by
364 performing bi-exponential curve fits to the observed frequency distribution of donor
365 fluorophore lifetimes, wherein one exponential component represents the population of
366 non-FRET monomeric donors and the other exponential component represents the
367 performance of the donors that are involved in FRET interactions.
368 First, we characterized the average lifetimes of unstimulated cells expressing several
369 configurations of fluorescent protein tagged Dectin-1A: 1) receptor with donor tag only,
370 2) co-expression of separate donor and acceptor tagged receptors with tags placed on
371 opposite sides of the plasma membrane (a negative control containing both fluorescent
372 proteins but in a configuration that does not permit FRET), and 3) co-expression of
373 separate donor and acceptor-tagged receptors with both tags in the cytoplasmic tail of
374 the receptors (configuration to be used for experimental determination of receptor
375 aggregation by FRET) (Fig. 5 B). The observed decay curves were analyzed by
376 performing a mono-exponential and bi-exponential fit. For donor only and our negative
377 control we observed a negative amplitude for the second component in the bi-
378 exponential fit, indicating a mono-exponential fit was superior for these conditions. This
379 was as anticipated since these conditions should have only a single, non-FRET donor

bioRxiv preprint doi: https://doi.org/10.1101/824995; this version posted May 25, 2020. The copyright holder for this preprint (which was not certified by peer review) is the author/funder, who has granted bioRxiv a license to display the preprint in perpetuity. It is made available under aCC-BY 4.0 International license.

signal. Additionally, the lifetimes of the second component in these controls unrealistically exceed >150 ns, further justifying a mono-exponential fit. Our results show that when acceptor is not present, we see the expected lifetime of 2.4 ns using a mono-exponential fit (Fig. 5B). Negative controls with donor and acceptor on opposite sides of the membrane yield similar lifetime values. Data from co-expression of cytosolic donor and acceptor-tagged receptor was fit bi-exponentially and the lifetime of both components is shown (Fig. 5B). We observed a decrease in the lifetime of the donor to 0.41 ns (FRET-involved second fit component of a bi-exponential fit) indicating that some basal level of intermolecular Dectin-1 close proximity interactions were being observed in unstimulated cells. Of course, the first fit component lifetime (non-FRET involved donors) remained at ~2.4 ns, as expected from controls above. The existence of this basal FRET signal is interesting, and the potential sources and interpretation of this observation are further considered below. However, we first focused on assessing ligation-dependent changes in Dectin-1A's molecular aggregation state as influenced by various glucans and measured by FRET. For the remainder of the FLIM-FRET experiments, we fixed the lifetime of the first component to 2.4 ns, and we showed the second components' lifetime and amplitude values as percentages, FRET Efficiency and Donor-Acceptor Population respectively.

When we stimulate cells expressing Dectin-1A with donor and acceptor on the cytoplasmic face of the membrane using MMW (Fig. 5D) or HMW (Fig. 5E) glucan, we see a significant increase in the fraction of receptors undergoing FRET (Donor-Acceptor population) from 15% before stimulation to a maximum of 30% after 5 minutes of stimulation, with this trend starting at about one minute post-stimulation. However, there

bioRxiv preprint doi: https://doi.org/10.1101/824995; this version posted May 25, 2020. The copyright holder for this preprint (which was not certified by peer review) is the author/funder, who has granted bioRxiv a license to display the preprint in perpetuity. It is made available under aCC-BY 4.0 International license.

403 is not a significant change in FRET efficiency before and after stimulation. On the other
404 hand, when we stimulate with LMW (Fig. 5C) or denatured MMW (Fig. 5F), we see no
405 significant change in FRET efficiency or donor-acceptor population. We interpret the
406 high and constant FRET efficiency for the population of receptors engaged in FRET
407 interactions to mean that Dectin-1A in its aggregated state is in a close configuration
408 (e.g., dimer or tetramer) that does not permit a wide range of separations between
409 donor and acceptor tags, leading to a constant FRET efficiency for the donor population
410 that does attain this FRET-capable configuration. However, the size of the population of
411 receptors engaged in these close molecular aggregates does change as a result of
412 stimulation with glucan. These results suggest that the highly structured soluble glucans
413 allow for an increase in Dectin-1A dimerization or oligomerization to occur, which
414 directly correlates with the amount of receptor activation and signaling observed.

bioRxiv preprint doi: https://doi.org/10.1101/824995; this version posted May 25, 2020. The copyright holder for this preprint (which was not certified by peer review) is the author/funder, who has granted bioRxiv a license to display the preprint in perpetuity. It is made available under aCC-BY 4.0 International license.

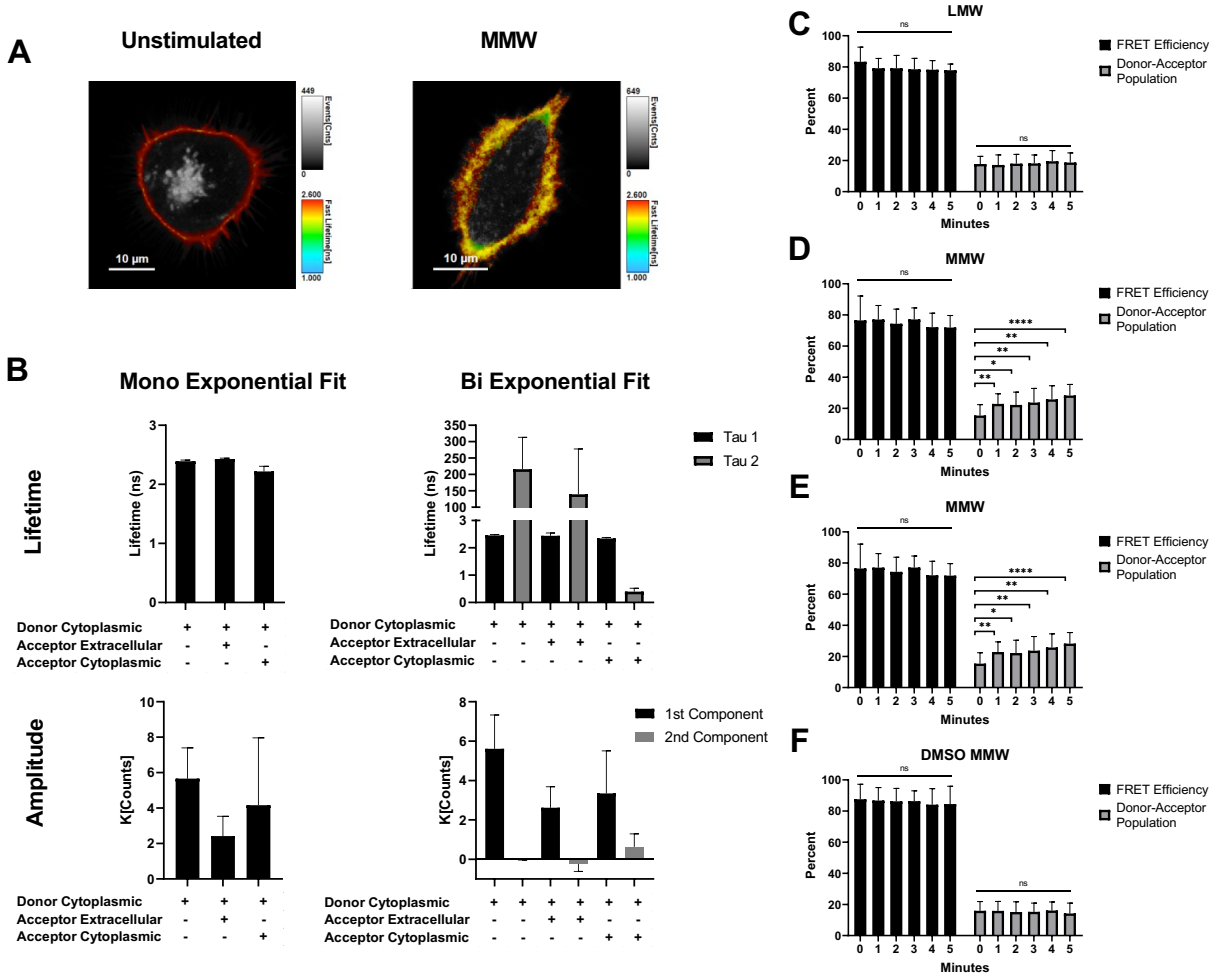

415

416 **Figure 5: Highly structured β-glucans induce dimerization/oligomerization of**

417 **Dectin-1A.**

418 (A) Representative average lifetime image of HEK-293 cell transfected with Dectin-1A-mEmerald or co-
419 transfected with Dectin-1A-mEmerald and Dectin-1A-mCherry. The analysis was conducted on the
420 plasma membrane by masking out internal cellular compartments on the images so only the masked
421 plasma membrane signal used for analysis is shown in color. In these images, pixel hue indicates raw
422 fluorescence lifetime over all populations observed and pixel intensity indicates total photon counts
423 observed over all populations. (B) Lifetime and amplitudes of HEK-293 cells expressing donor only on the
424 cytoplasmic face, donor expressed on the cytoplasmic side and acceptor on the extracellular side or
425 donor and acceptor placed on the cytoplasmic side of the membrane. Fluorescence decay curves were
426 mono- and bi-exponentially fit and individual fit components are shown. Data shown as mean ± SD (n =

bioRxiv preprint doi: https://doi.org/10.1101/824995; this version posted May 25, 2020. The copyright holder for this preprint (which was not certified by peer review) is the author/funder, who has granted bioRxiv a license to display the preprint in perpetuity. It is made available under aCC-BY 4.0 International license.

15 cells). (C-F) FRET efficiency and Donor-Acceptor Population of cells stimulated with LMW (C), (D) MMW, (E) HMW, or (F) DMSO denatured MMW glucan. Data shown as mean ± SD (n = 15); One-way ANOVA with multiple comparisons by the Dunnett test, * $p<0.05$, ** $p<0.01$, *** $p<0.001$.

In addition, to better characterize the aggregation states accessible to Dectin-1A, we conducted a Number and Brightness analysis (N&B) on HEK-293 cells expressing Dectin-1A-mEmerald. Previous research has described N&B more in depth [60–62]. Briefly, N&B analysis focuses on fluctuation of detected emission photons originating from fluorescent molecules that pass through a known observation volume. Statistics of fast fluctuations of the intensity at each pixel can be used to determine the number and intensity of the particles diffusing through the observation volume. For example, if the fluorescent proteins diffuse as a tetrameric protein, we expect to observe emission intensity fluctuation with four times more photons relative to a monomeric fluorescent protein diffusing through the excitation volume. Receptor aggregation was observed by stimulating these cells with soluble glucans. A brightness vs intensity 2D histogram of each pixel in a time series was developed and selection boxes were drawn to represent monomers (red box), dimers (green box) and oligomers (blue box) (greater than dimer; Fig. 6A). Dectin-1 aggregation state maps of representative untreated (Fig. 6B) and MMW-stimulated cells (Fig. 6C) were generated using this color scheme. Our results indicated that unstimulated and LMW stimulated cells contained a significantly higher amount of monomer pixels compared to MMW and HMW glucan treated cells (Fig. 6D). Inversely, we observed a significant increase in pixels with a dimer and oligomer brightness in cells stimulated with MMW and HMW compared to cells that were

bioRxiv preprint doi: https://doi.org/10.1101/824995; this version posted May 25, 2020. The copyright holder for this preprint (which was not certified by peer review) is the author/funder, who has granted bioRxiv a license to display the preprint in perpetuity. It is made available under aCC-BY 4.0 International license.

unstimulated or LMW stimulated (Fig. 6E, F). N&B analysis revealed that dimers of Dectin-1A account for the majority of aggregated state Dectin-1.

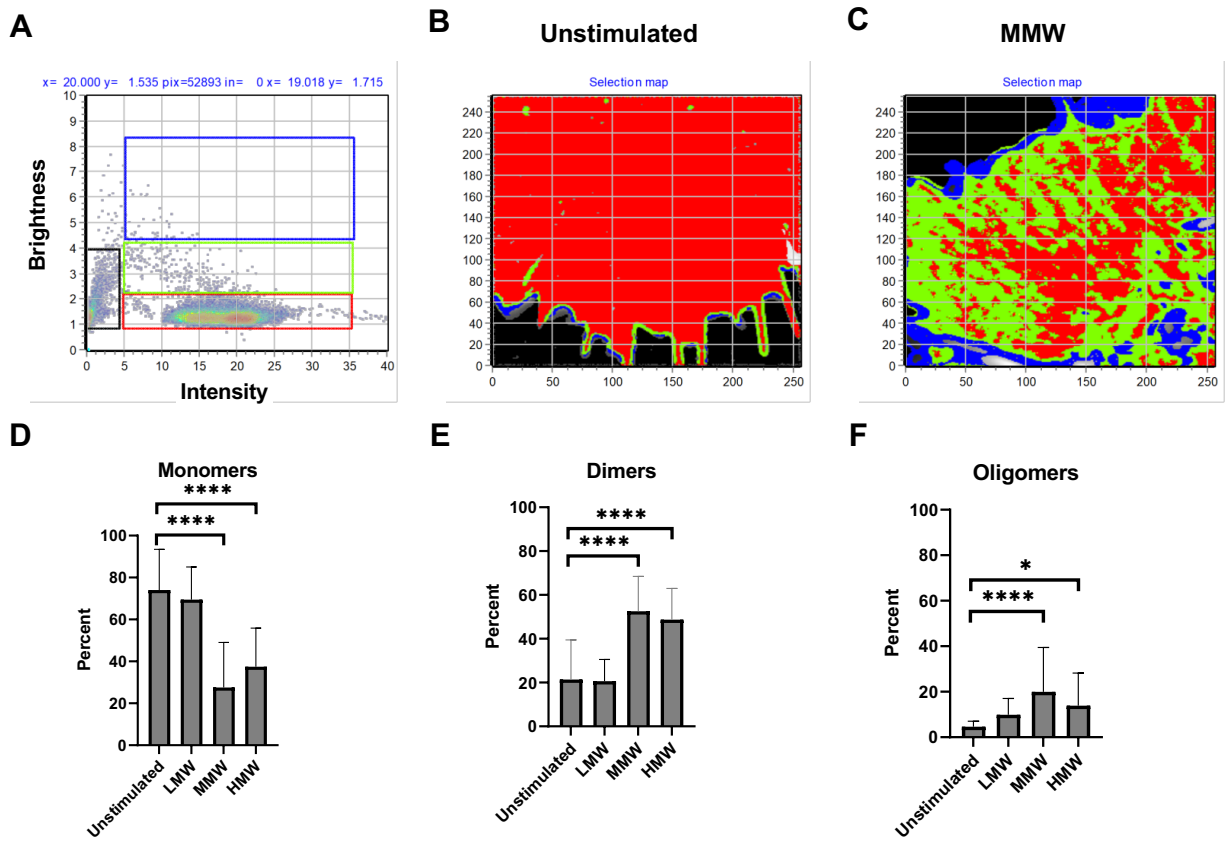

Figure 6: Number and Brightness analysis shows formation of small oligomeric states of Dectin-1A when stimulated with highly structured β-glucans.

(A) Brightness vs intensity 2D histogram shows the selected pixels that contribute to the background (black), monomers (red), dimers (green), and oligomers (blue) in the image. (B) Representative selection map of HEK-293 cells expressing Dectin-1A-mEmerald shows receptor aggregation in unstimulated cells or those stimulated with (C) MMW β-glucan. Dectin-1 aggregation states are defined by colored boxes selected in the Brightness vs intensity histogram. (D,E,F) Percentage of (D) monomers, (E) dimers, and (F) oligomers in Dectin-1A-mEmerald receptors and receptor ligand complexes obtained from N&B analysis before or after stimulation. Data shown as mean ± SD (n = 30); One-way ANOVA with multiple comparisons by the Dunnett test, * $p<0.05$, **** $p<0.00001$.

bioRxiv preprint doi: https://doi.org/10.1101/824995; this version posted May 25, 2020. The copyright holder for this preprint (which was not certified by peer review) is the author/funder, who has granted bioRxiv a license to display the preprint in perpetuity. It is made available under aCC-BY 4.0 International license.

β-glucan induced Dectin-1A aggregates are below 15 nm in size

While FRET-based observations and N&B analysis clearly show the presence of ligand-induced, molecular-scale aggregation (e.g., dimerization) of Dectin-1A, these methods are not as well suited to discern the existence of larger scale aggregation of the receptor (e.g., clusters of tens to hundreds of receptors). We used direct Stochastic Optical Reconstruction Microscopy (dSTORM) coupled with Hierarchical Single-Emitter hypothesis Test (H-SET) analysis [13] to resolve aggregation of Dectin-1A before and after stimulation with MMW glucan. This localization super resolution microscopy technique accurately resolves objects from the diffraction limit (~300 nm, the resolution limit of conventional fluorescence microscopy methods) or above, down to ~15 nm (a typical resolution limit of dSTORM using our configuration). H-SET analysis detected sites of Dectin-1 labeling as “singlet” objects or “multiple” clustered objects. Multiple clustered objects are those with three or more resolvable individual Dectin-1 molecules. Singlet objects are those that appear to contain only a single, resolvable Dectin-1 labeling event, though it is possible that multiple Dectin-1 molecules in very close proximity (<15 nm separation) would be unresolvable and appear as a singlet object. We detected no significant change in the density of singlet objects or multiple object clusters before vs after MMW glucan stimulation (Fig. 7A,B; Supplemental Fig. 2). Consistent with a Dectin-1 distribution of predominantly monomers or low order oligomers (likely unresolvable by dSTORM), singlet exposures greatly outnumber multiple exposures on the cell wall surface (Fig. 7C). Localization number per multiple cluster object did not change with stimulation (Supplemental Fig. 2), suggesting no

bioRxiv preprint doi: https://doi.org/10.1101/824995; this version posted May 25, 2020. The copyright holder for this preprint (which was not certified by peer review) is the author/funder, who has granted bioRxiv a license to display the preprint in perpetuity. It is made available under aCC-BY 4.0 International license.

change in the number of receptors in this minority population of Dectin-1. In the context of the previous findings showing molecular aggregation at very small scales, potentially below the resolution limit of dSTORM, we concluded that dSTORM results indicated that the Dectin-1A aggregates formed upon glucan stimulation are quite small and remain below the resolution limit of dSTORM (<15 nm length scale). Because this places an upper bound on the size of ligand-induced Dectin-1 clusters and we can estimate that the CRD of Dectin-1 occupies an area approximately 25 nm^2 (PDB: 2BPD; [57,63]), we conclude that Dectin-1 aggregation after MMW glucan stimulation most likely involves collections of not more than ~7 receptors.

bioRxiv preprint doi: https://doi.org/10.1101/824995; this version posted May 25, 2020. The copyright holder for this preprint (which was not certified by peer review) is the author/funder, who has granted bioRxiv a license to display the preprint in perpetuity. It is made available under aCC-BY 4.0 International license.

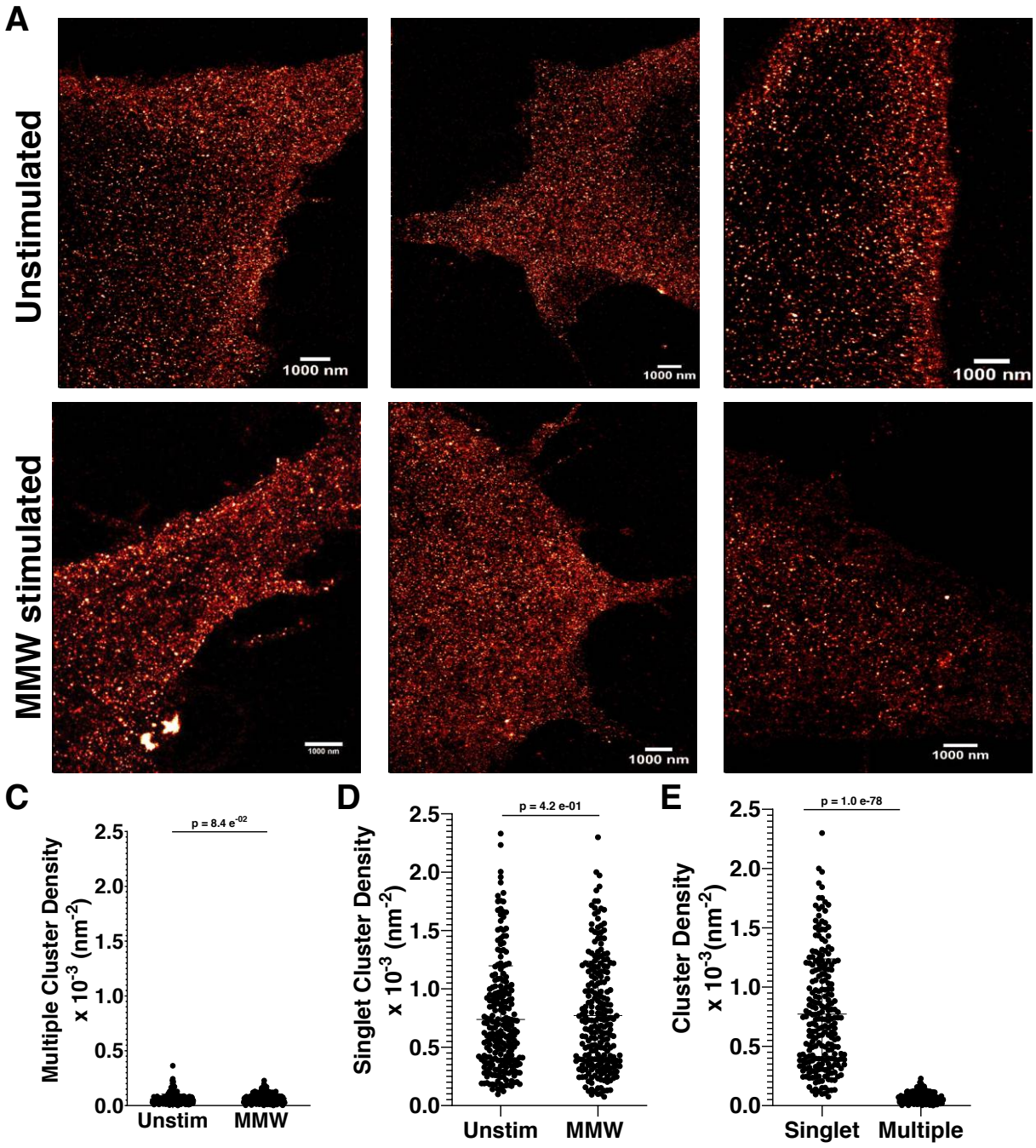

Figure 7: Dectin-1A does not form large scale aggregates when stimulated with highly structured β-glucan.

bioRxiv preprint doi: https://doi.org/10.1101/824995; this version posted May 25, 2020. The copyright holder for this preprint (which was not certified by peer review) is the author/funder, who has granted bioRxiv a license to display the preprint in perpetuity. It is made available under aCC-BY 4.0 International license.

(A) Representative immunofluorescence staining images of HEK-293 cells expressing Dectin-1A and either unstimulated or stimulated with MMW β-glucan. Cells were stained with a conjugated anti-Dectin-1-Alexa 647 antibody. (B) Multiple cluster density of dSTORM analysis of HEK-293 cells expressing Dectin-1A unstimulated or stimulated for 50 sec with MMW glucan. (C) Singlet cluster density of dSTORM analysis of HEK-293 cells expressing Dectin-1A unstimulated or stimulated for 50 sec with MMW glucan. (D) Cluster density of singlet and multiple exposure of Dectin-1A expressing HEK-293 cells treated for 50 sec with MMW glucan. Data shown as mean ± SD (n = 34) with significance assessed by Student's T Test.

Dectin-1A is predominantly monomeric in resting cell membranes

FRET-based measurements and N&B analysis reported that the large majority of Dectin-1 is distributed as monomers in unstimulated cells. However, a minority population of apparent close-proximity receptor states was observed in resting cells by both techniques. This may represent density-dependent, close-proximity interactions between Dectin-1 molecules driven by random collisional interactions, without necessarily requiring receptor oligomer formation. Alternatively, it is possible that a small fraction of Dectin-1 does form low order oligomers, even in the absence of glucan. It is difficult to conclusively distinguish between these alternative hypotheses using only the experimental results shown above. Therefore, we created a computational model of fully monomeric Dectin-1 undergoing Brownian 2D diffusion. If such a model could predict collisional FRET interactions at a level consistent with our FRET observations in resting cells, we would conclude that random collisional interactions are sufficient to explain basal FRET observed for Dectin-1 in this study. To accurately parameterize this model, we determined the receptor density of both donor and acceptor for HEK-293 cells coexpressing Dectin-1A mEmerald/mCherry by RICS analysis (Fig. 8A). Our

bioRxiv preprint doi: https://doi.org/10.1101/824995; this version posted May 25, 2020. The copyright holder for this preprint (which was not certified by peer review) is the author/funder, who has granted bioRxiv a license to display the preprint in perpetuity. It is made available under aCC-BY 4.0 International license.

results indicated on average Dectin-1 cotransfected cells contain 54.6% mEmerald and 45.4% mCherry (Fig. 8B). Therefore, our model was populated by equal proportions of donor and acceptor tagged Dectin-1 molecules. Their diffusion coefficients were parameterized using data from Fig. 4. The model calculated FRET rates for all donor-acceptor pairs within a specified maximum radial distance. The maximum radius for experimental FRET observation is limited by signal-to-noise ratio and other factors. To avoid simulating FRET measurements at experimentally unrealistic radii, we varied the model's maximum donor-acceptor radial distance for FRET calculations in a range of 4-10 nm. We compared simulated and experimental FRET efficiencies and used maximum radii for simulations that yielded FRET efficiency in best agreement with observed FRET efficiency on resting cells, indicating comparable "sensitivity" of FRET detection in both. Our results show our experimental FRET efficiency values match model predictions closely at maximum radii between 5 and 6 nm (Fig. 8C). Simulations at these chosen parameters were then compared to experimental results with respect to the donor-acceptor population percent that they predicted.

We used the predictions of this computational model to test the hypothesis that random collisional FRET interactions of donors and acceptors is sufficient to explain the basal FLIM-FRET signal observed experimentally in resting cells. If this model, which incorporates only collisional interactions between donors and acceptors, predicts a percent of donors undergoing FRET interactions with acceptors that match the experimentally observed value, we would consider that collisional interactions alone are sufficient to explain the observed basal FRET signal. However, if the model predicts a value significantly below that experimentally observed, we would propose that a minor

bioRxiv preprint doi: https://doi.org/10.1101/824995; this version posted May 25, 2020. The copyright holder for this preprint (which was not certified by peer review) is the author/funder, who has granted bioRxiv a license to display the preprint in perpetuity. It is made available under aCC-BY 4.0 International license.

547 fraction of Dectin-1 molecules may participate in oligomeric aggregates on cell
548 membranes, even in the absence of glucan. Using simulations with maximum radial
549 values of 5 and 6 nm, our results indicate that the experimentally observed amount of
550 Dectin-1 receptors dimerizing (Donor-Acceptor population) prior to stimulation match
551 closely to our simulated results (Fig. 8D). This indicated that the FRET signal we
552 observe prior to stimulation was attributable to random “collisional” interactions of
553 Dectin-1A at the level of expression present in our experimental system.

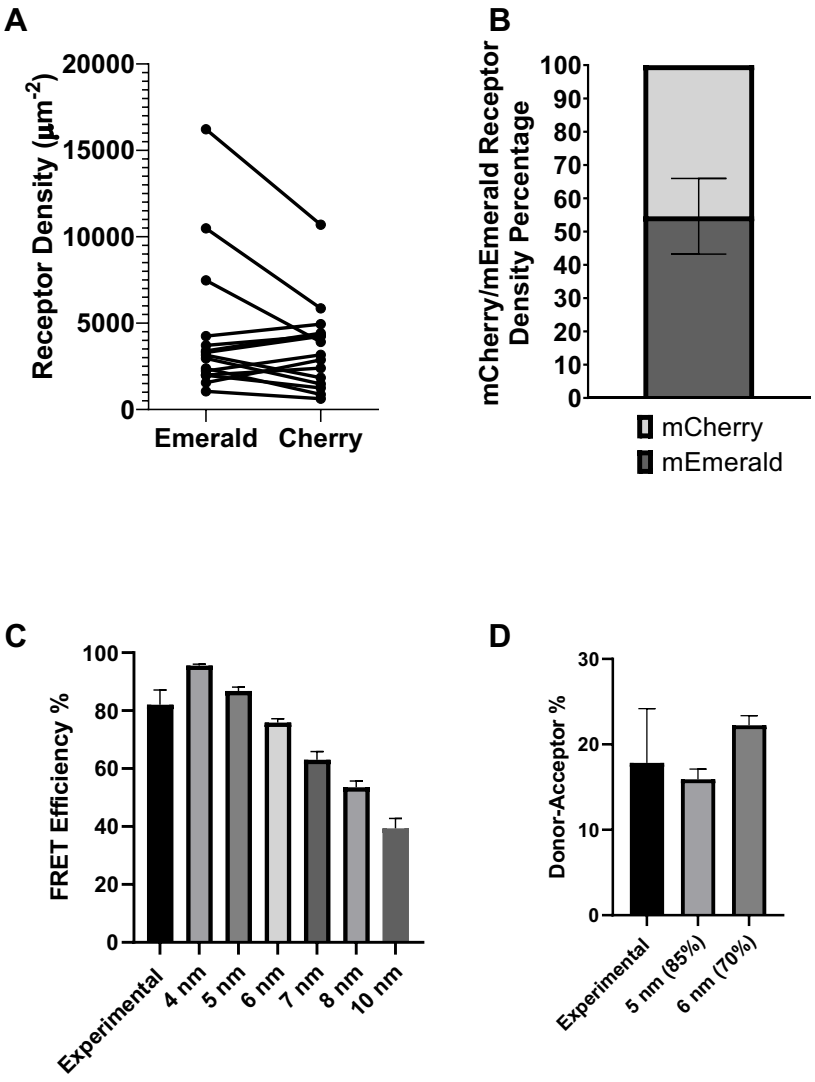

554

bioRxiv preprint doi: https://doi.org/10.1101/824995; this version posted May 25, 2020. The copyright holder for this preprint (which was not certified by peer review) is the author/funder, who has granted bioRxiv a license to display the preprint in perpetuity. It is made available under aCC-BY 4.0 International license.

Figure 8. Computational FRET modeling of monomeric Dectin-1A can account for basal FRET observed in Dectin-1A expressing cells.

(A) Receptor density of HEK-293 cells co-expressing Dectin-1A-mEmerald and -mCherry. Lines connect paired readings from single cells. (B) Ratio of mEmerald/mCherry expression in unstimulated HEK-293 cells. (C) FRET Efficiency of Dectin-1A donor/acceptor-containing computational models at different maximum intermolecular radial distances and experimental observations of FRET efficiency in resting cells for comparison. To facilitate comparison, model FRET Efficiencies are averaged over only the donors participating in non-zero FRET efficiency interactions with acceptors, and experimental FRET efficiency is derived from aggregation of all unstimulated ("0 minute") cell data depicted in Fig. 5C-F. (D) Percentage of donors undergoing FRET (Donor-Acceptor Population) for experimentally observed populations in unstimulated cells and computational FRET modeling data at 5 and 6 nm maximum FRET radii. Experimental FRET donor-acceptor percentages were derived from aggregation of all unstimulated ("0 minute") data in Fig. 5C-F. Data shown as mean ± SD (n = 15 independent simulations or experimental observations on cells, respectively); One-way ANOVA multiple comparisons Dunnett test.

Dectin-1A dimer/oligomer and contact site formation is more efficient with cells incubated with *C. albicans* containing high glucan exposure.

Throughout the article, we have focused on experiments using soluble glucans. In order to show Dectin-1 aggregation occurs during fungal pathogen recognition, we used a high (TRL035) and low (SC5314) β-glucan exposing *C. albicans* yeast and examined Dectin-1 aggregation occurring at the contact sites. TRL035 has been previously shown to have high glucan exposure compared to SC5314 [64]. In addition, our representative images show TRL035 forming a phagocytic cup more efficiently than SC5314 (Fig. 9A). Our results show that HEK-293 cells co-transfected with Dectin-1A-mEmerald and Dectin-1A-mCherry exhibit an increase in the proportion of aggregated-state receptors

bioRxiv preprint doi: https://doi.org/10.1101/824995; this version posted May 25, 2020. The copyright holder for this preprint (which was not certified by peer review) is the author/funder, who has granted bioRxiv a license to display the preprint in perpetuity. It is made available under aCC-BY 4.0 International license.

580 from approximately 15% in non-contact site membrane to about 25% in contact sites of
581 high glucan exposing yeast TRL035 and *C. albicans* derived glucan particles.
582 Interestingly, we did not measure a significant increase in receptor aggregation between
583 non-contact membranes and contact sites with low glucan exposing SC5314 (Fig. 9
584 B,C), which may indicate that the amount of aggregated Dectin-1 at SC5314 contacts
585 was quite small and below the detection limit. Furthermore, we observed no significant
586 difference in FRET efficiency between any conditions tested (Fig. 9B), similarly to our
587 observations with soluble glucan. The significance and interpretation of these findings is
588 further discussed below. These results suggest that the larger cell wall glucan exposure
589 results in an increase of Dectin-1 in molecular aggregates with associated signaling,
590 resulting in a more efficient recognition of yeast by the Dectin-1A receptor.

bioRxiv preprint doi: https://doi.org/10.1101/824995; this version posted May 25, 2020. The copyright holder for this preprint (which was not certified by peer review) is the author/funder, who has granted bioRxiv a license to display the preprint in perpetuity. It is made available under aCC-BY 4.0 International license.

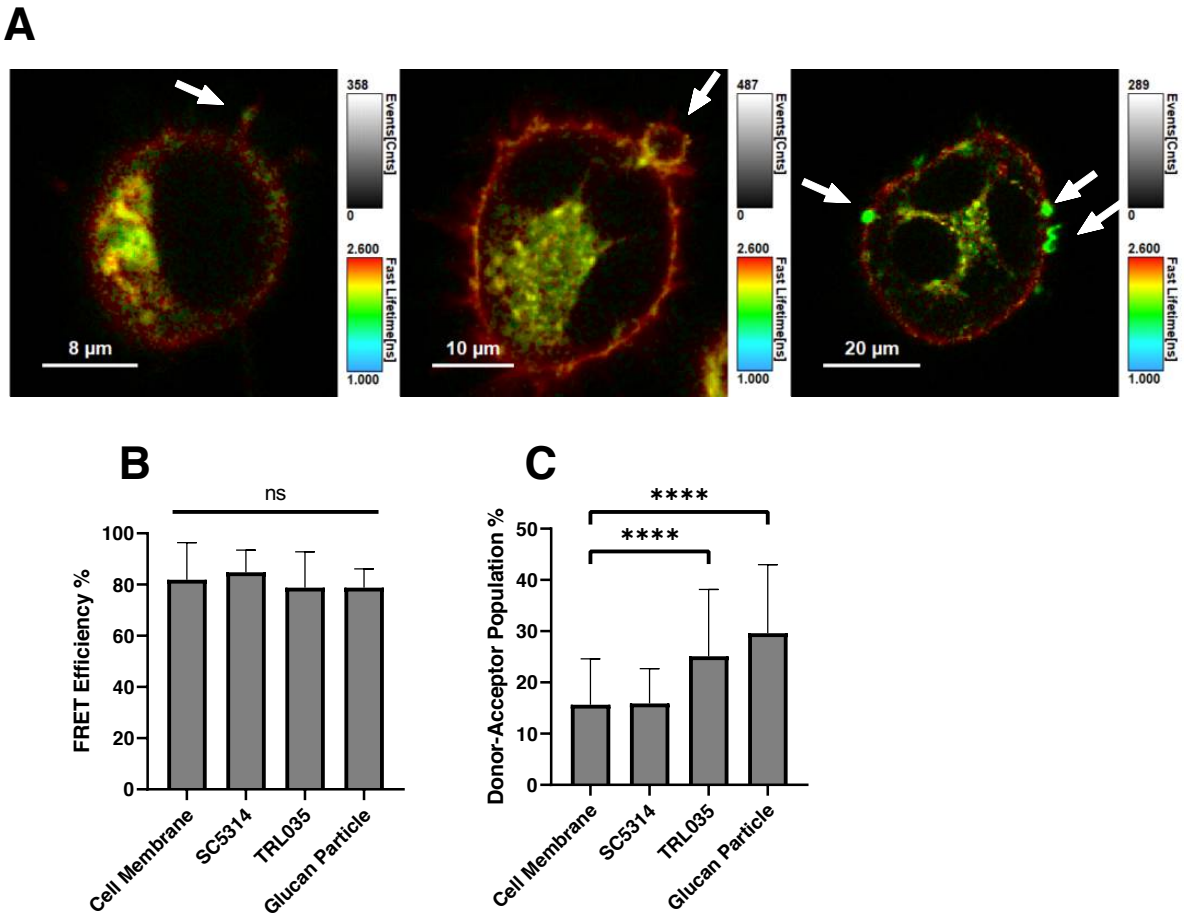

591

592 **Figure 9: Dectin-1A forms more oligomers at fungal contact sites with high β-**

593 **glucan exposure.**

594 (A) Representative lifetime images of HEK-293 cells co-transfected with Dectin-1A-mEmerald and Dectin-

595 1A-mCherry incubated with SC5314 (left panel), TRL035 (middle panel) or particulate glucan (right

596 panel). Transition from redder to greener pixels at contact sites is indicative of increased FRET

597 interactions between Dectin-1 receptors. In these images, pixel hue indicates raw fluorescence lifetime

598 over all populations observed and pixel intensity indicates total photon counts observed over all

599 populations. (B) FRET efficiency and (C) donor-acceptor population of cell membranes with no fungal

600 contact, SC5314 (low glucan exposure), TRL035 (high glucan exposure), or particulate glucan. Data

601 shown as mean ± SD (n = 15); One-way ANOVA with multiple comparisons by the Dunnett test, ****

602 $p<0.00001$.

bioRxiv preprint doi: https://doi.org/10.1101/824995; this version posted May 25, 2020. The copyright holder for this preprint (which was not certified by peer review) is the author/funder, who has granted bioRxiv a license to display the preprint in perpetuity. It is made available under aCC-BY 4.0 International license.

Discussion

Our results demonstrate that the structure of β-glucan impacts receptor signaling by determining the membrane organization and molecular aggregation state of Dectin-1A. We showed that glucans with higher order structure are better able to activate Dectin-1A signaling. Upon activation by stimulatory soluble glucan, Dectin-1A enters aggregated states that contain dimers and higher order oligomers, but these appear to remain as small nanoscale domains containing relatively small numbers of receptors. Comparison of computational modeling and experimental FLIM-FRET data confirms that Dectin-1A exists in a monomeric state in resting cells. Further, monomeric receptors oligomerize and aggregate in a fashion that is dependent upon glucan higher order structure and correlated with the magnitude of membrane proximal signaling downstream of Dectin-1. Finally, we observed that a similar process of increasing Dectin-1 aggregation is seen at contact sites with yeast and fungal-derived particles, and that the amount of aggregated state Dectin-1A correlates with the degree of glucan exposure on the surface of the particle.

The prevalence of ensemble based studies of biological response to fungal glucans, using glucans from varying sources and with varying degrees of structural characterization, has complicated a thorough understanding of the impact of glucan physicochemical properties on their biological activity. Innate immunocytes are naturally exposed to β-glucan in both particulate and soluble forms. β-glucan is widely distributed on various fungal species as an insoluble component of the cell wall. The soluble form is produced when macrophages recognize fungal surfaces and release

bioRxiv preprint doi: https://doi.org/10.1101/824995; this version posted May 25, 2020. The copyright holder for this preprint (which was not certified by peer review) is the author/funder, who has granted bioRxiv a license to display the preprint in perpetuity. It is made available under aCC-BY 4.0 International license.

626 enzymes that degrade cell wall glucans [46,47]. These soluble glucans are commonly
627 found in circulation in the serum of patients with fungal infections [48,49]. Low molecular
628 weight glucans typically possess a random coil structure while increasing single or triple
629 helical structure is generally seen as molecular weight increases [65]. In general,
630 complexity of β-glucan correlates with immunostimulatory potency [17,27,29,65,66].
631 Mueller, et al indicated a correlation between glucan triple helical structure and binding
632 affinity for receptors on human promonocytic cells, which is contrary to our finding of
633 similar affinity across glucans tested herein [27]. Discrepancies in the impact of glucan
634 structure on affinity may be due to different cell backgrounds, or more likely, to the fact
635 that Mueller, et al used glucans from a wide range of sources, with complex differences
636 in structure not merely limited to size or helical content. Our study used a carefully
637 characterized series of fungal glucans to determine that Dectin-1A activation is
638 specifically influenced by the degree of β-glucan triple helical structure, not merely
639 through its affinity or size. Furthermore, the single-cell nature of our observations
640 suggests that the biological response to glucans with strong helical structure (e.g.,
641 HMW glucan) seems bi-stable in nature, with response/non-response being correlated
642 with glucan structure but the amplitude of calcium signal being similar in single cells,
643 once successfully triggered.
644 Aggregate states of Dectin-1 relevant to signaling could exist in a pre-formed, ligation-
645 independent state, be formed in a purely ligation-dependent manner, or a mixture of
646 both models. We entertained the possibility of pre-formed aggregates because receptor
647 oligomeric states exist in the basal state for some other C-type lectin receptors, such as
648 DCSIGN, DNGR-1, and NKp80 [67–70]. However, Dectin-1A does not contain cysteine

bioRxiv preprint doi: https://doi.org/10.1101/824995; this version posted May 25, 2020. The copyright holder for this preprint (which was not certified by peer review) is the author/funder, who has granted bioRxiv a license to display the preprint in perpetuity. It is made available under aCC-BY 4.0 International license.

649 residues in its stalk region which are important in the dimerization of some other C-type
650 lectin receptors (i.e., DNGR-1). Comparison of FRET data and computational modeling
651 results demonstrated that any FRET activity observed in resting cells was explainable
652 by expected levels of transient collisional donor-acceptor interactions in our cells. N&B
653 analysis independently confirmed that the large majority of Dectin-1 is in monomeric
654 states prior to stimulation. Therefore, we concluded that Dectin-1 is unlikely to undergo
655 significant dimerization/oligomerization prior to ligation by glucan.
656 We proceeded to test the hypothesis Dectin-1 undergoes ligation-dependent
657 aggregation. Specifically, we investigated whether glucan structure impacts signaling by
658 modulating the frequency of Dectin-1A dimer/oligomer formation. Dectin-1
659 dimerization/oligomerization would create sites where Syk could be better recruited via
660 interactions of its SH2 domains with the (hem)ITAM phosphorylated YXXL sequence in
661 closely juxtaposed Dectin-1A cytosolic tails. In fact, this model is commonly cited in
662 review literature in the field, but direct evidence in intact, live cells has been lacking
663 [71,72]. The plausibility of the Dectin-1 (hem)ITAM aggregation model is suggested by
664 the fact that another C-type lectin receptor, CLEC-2, forms a minimal signaling unit
665 composed of a phosphorylated dimer, enabling recruitment of a single molecule of Syk
666 [44]. Our FLIM-FRET and N&B results reveal that Dectin-1A enters a state of greater
667 molecular aggregation when stimulated with β-glucans, and that the degree of glucan
668 helical structure correlates with its ability to induce Dectin-1 aggregation. FRET and
669 N&B are very sensitive methods to identify receptor aggregation on the scale of small
670 oligomers, but these methods are limited in their ability to distinguish such small
671 aggregates from the formation of larger receptor nanodomains. dSTORM failed to

bioRxiv preprint doi: https://doi.org/10.1101/824995; this version posted May 25, 2020. The copyright holder for this preprint (which was not certified by peer review) is the author/funder, who has granted bioRxiv a license to display the preprint in perpetuity. It is made available under aCC-BY 4.0 International license.

detect ligand inducible Dectin-1 nanodomains on a length scale of ≥15 nm, suggesting that Dectin-1 aggregation events are limited to small collections of ≤7 receptors. Our core observation of ligation-inducible Dectin-1 aggregation is directly in line with previous crystallographic studies that show monomeric Dectin-1A CRD in the absence of glucan but able to form dimeric complexes in the presence of β-glucan [57]. In addition, solution biophysical studies have shown a ligand-induced cooperative formation of Dectin-1 CRD tetramers (or dimers of dimers) [57,58]. However, these studies were performed with truncated receptor ectodomain proteins outside the context of living cell membranes, so our findings better establish and define the relevance of ligation-dependent Dectin-1 aggregation in a more physiologically realistic context. Nanoscale glucan exposures on *Candida* cell wall surfaces may be important determinants of the degree of Dectin-1 aggregation at host-pathogen contact sites [13,64]. Dectin-1 is recruited to the "phagocytic synapse" between innate immunocytes and fungal particles. Here, Dectin-1A encounters fungal glucan and initiates signaling [73]. We have previously described that *C. albicans* TRL035 exhibits larger glucan nanoexposures than *C. albicans* SC5314 [64]. Consistent with the presence of larger glucan exposures, we observed greater Dectin-1 aggregation at FRET contact sites with TLR035, relative to SC5314. Cell wall glucan nanoexposures are larger (~20-200 nm) than the Dectin-1 aggregates generated by soluble glucans in the present work. Therefore, future studies could productively investigate the role of glucan nanoexposures in stabilizing larger aggregated collections of engaged Dectin-1, and the potential dependence of cellular activation on the scale of Dectin-1 aggregation at sites of cell wall glucan nanoexposures.

bioRxiv preprint doi: https://doi.org/10.1101/824995; this version posted May 25, 2020. The copyright holder for this preprint (which was not certified by peer review) is the author/funder, who has granted bioRxiv a license to display the preprint in perpetuity. It is made available under aCC-BY 4.0 International license.

These and other studies improve our physical understanding of host-*Candida* interaction and highlight the exquisite sensitivity of the Dectin-1 system that drives innate immune fungal recognition. Our previous optical nanoscopy studies of *Candida* cell wall surfaces estimated multivalently-engaging glucan exposure site density and area (per exposure site) as follows: SC5314—1 μm^{-2} density, $6.61x10^{-4}$ μm^2 area; TRL035—4 μm^{-2} density, $9.62x10^{-4}$ μm^2 area [64]. The total area of contact sites between *C. albicans* and human immature dendritic cells is ~10 μm^2 [74]. Finally, we estimate (see above) that one Dectin-1 CRD occupies a footprint of ~25 nm^2. From these figures, we calculate that a typical phagocytic synapse would contain a maximum of 264 multivalently engaged Dectin-1 proteins for *C. albicans* SC5314, and maximum 385 multivalently engaged Dectin-1 for TRL035 (at total ligand engagement). Based on our reported Dectin-1 density (Fig. 4), the contact sites we measured would contain ~46000 total Dectin-1 proteins. So, the Dectin-1 system is able to drive signaling responses when, at most, only a few hundred receptors, corresponding to less than 1% of the total contact site resident Dectin-1 proteins, are aggregated in the contact. These results and estimates suggest that fungal recognition requires the Dectin-1 system to engage in a search for rare sites of multivalent interaction with glucan. Signal initiation must be sensitive to activation of relatively small numbers of Dectin-1 proteins. In the future, it will be important to achieve a better understanding of Dectin-1's collaboration with other anti-fungal receptors (e.g., DC-SIGN and CD206). Such receptors may be important for building and stabilizing a fungal contact that can effectively promote Dectin-1's ability to search for and find its rare sites of glucan exposure.

bioRxiv preprint doi: https://doi.org/10.1101/824995; this version posted May 25, 2020. The copyright holder for this preprint (which was not certified by peer review) is the author/funder, who has granted bioRxiv a license to display the preprint in perpetuity. It is made available under aCC-BY 4.0 International license.

Overall, these findings indicate that β-glucan structure is required for Dectin-1A to undergo Syk-dependent signaling. Here we provide evidence in support of a model in which highly structured glucans induce stable dimerization and/or oligomerization of the receptor. This allows their (hem)ITAM domains to become close enough for a sufficient period of time to allow for the activation of Syk, leading to further signaling cascades. Greater understanding of receptor activation is required to better understand the role of Dectin-1A and its agonists as a potential way forward for adjuvant and immunotherapy development. Furthermore, given the worldwide burden of candidiasis, further experimentation is required to better understand the role of Dectin-1A in recognition of these pathogens.

Materials and Methods

Cell Culture

The HEK-293 (ATCC, #CRL-1573) cell line was maintained in Dulbecco's Minimum Essential Medium supplemented with 10% Fetal Bovine Serum (FBS), 1% penicillin/strepromycin, 2mM L-glutamine, 11mM sodium pyruvate, and 1% HEPES. Cells were grown in an incubator at 37°C at 5% CO_2 and saturating humidity. Cells were maintained at 37°C, 5% CO_2, and 75% relative humidity during imaging.

Plasmids and Transfection of Dectin-1 Constructs

Emerald-Dectin1A-N-10(Addgene plasmid, #56291), Emerald-Dectin1A-C-10 (Addgene plasmid # 54057), mCherry-Dectin1A-C-10 (Addgene plasmid # 55025), and mCherry-Dectin1A-N-10 (Addgene plasmid # 55026) was a gift from Michael Davidson. pUNO1-hDectin-1A (Invivogen) was stably transfected into HEK-293 cells for use in our calcium

bioRxiv preprint doi: https://doi.org/10.1101/824995; this version posted May 25, 2020. The copyright holder for this preprint (which was not certified by peer review) is the author/funder, who has granted bioRxiv a license to display the preprint in perpetuity. It is made available under aCC-BY 4.0 International license.

740 studies. Stable transfection of mEmerald-Dectin-1A was used for Syk immunoblotting
741 experiments. To generate stable lines, HEK-293 cells expressing either mEmerald-
742 Dectin-1A or pUNO-hDectin-1A were selected using Geneticin (G418 Sulfate) (Thermo-
743 Fischer, #10131035) at 400 µg/ml or Blasticidin (Santa Cruz Biotechnology, #SC-
744 495389) at 20 µg/ml, respectively, for 2 weeks.
745 All other experiments involving exogenous protein expression used transient
746 transfection. Transient transfection with plasmids was performed using standard
747 manufacturer protocols with Fugene 6 (Promega, #E2691).
748 **Fungal Growth/Preparation**
749 *C. albicans* SC5314 (ATCC, MYA-2876) or TRL035 yeast cells were grown from
750 glycerol stock, stored at −80°C. Samples were grown in YPD, for 16 h at 37°C in an
751 orbital shaker at 250 rpm to mid log phase. Following a 3-minute centrifugation at 6000
752 rpm, the supernatant was removed, and the cells were resuspended in 4%
753 paraformaldehyde and sterile phosphate-buffered saline (PBS) for 15 minutes. The cells
754 were centrifuged and washed with sterile PBS three times. The cell concentration was
755 then determined using a disposable hemocytometer (C-Chip; Bulldog Bio catalog no.
756 DHC-N01). 3.5 x10^6 cells were resuspended in 1 ml of PBS. 100 µl of the solution was
757 added to HEK-293 cells in 35 mm dishes 15 minutes prior to imaging.
758 **Glucan Particles**
759 Glucan microparticles were prepared from lyophilized *C. albicans* SC5314 yeast derived
760 from stationary phase culture in YPD. Dry yeast were extracted thrice in boiling 0.75N
761 NaOH (15 min), then residue was extracted thrice in boiling 2N H_3PO_4 (15 min), then
762 residue was extracted thrice in boiling acidic ethanol (1% v/v H_3PO_4 in ethanol; 15 min),

bioRxiv preprint doi: https://doi.org/10.1101/824995; this version posted May 25, 2020. The copyright holder for this preprint (which was not certified by peer review) is the author/funder, who has granted bioRxiv a license to display the preprint in perpetuity. It is made available under aCC-BY 4.0 International license.

and residue slurry was adjusted to neutral pH and washed thrice with ultrapure water. Pyrogen free reagent and glassware was used throughout preparation, and particles were stored at 4°C in sterile, pyrogen free water.

Soluble Glucan Chromatographic Analysis

Low (LMW, 11 kDa), medium (MMW, 145 kDa), and high (HMW, 450 kDa) molecular weight β-(1,3;1-6)-glucan extracted from *S. cerevisiae* cell wall was obtained from ImmunoResearch Inc. (Eagan, MN). The molecular weight was assessed by gel permeation chromatography (GPC) and multi-angle light scattering (MALS). Samples (100 µg) were injected and eluted with a mobile phase of 0.15 M sodium chloride containing 0.02% sodium azide at a flow rate of 0.5 mL/min using two Waters Ultrahydrogel 500 columns and one Waters Ultrahydrogel 250 column connected serially. The samples were run with the column temperature at 18°C. The Mw was calculated using Wyatt Astra software using data resulting from measurements of the angular variation of scattered light using the MALS detector coupled with the concentration measured by the refractive index signal.

Soluble Glucan Linkage Analysis

Desalted and lyophilized samples of the fractions were dissolved in dimethylsulfoxide (DMSO) and treated with NaOH and methyl iodide to methylate all free hydroxyl groups [75]. The methylated material was purified by extraction with dichloromethane and washing with water. The purified material was then hydrolyzed with trifluoroacetic acid, the reducing ends of the resulting sugars were reduced with $NaBD_4$, and then the resulting free hydroxyl groups were acetylated with acetic anhydride. The mixture of partially methylated alditol acetates was analyzed by gas chromatography. Each

bioRxiv preprint doi: https://doi.org/10.1101/824995; this version posted May 25, 2020. The copyright holder for this preprint (which was not certified by peer review) is the author/funder, who has granted bioRxiv a license to display the preprint in perpetuity. It is made available under aCC-BY 4.0 International license.

derivative corresponding to a particular linkage has been identified by a characteristic retention time and mass spectrum using a mass detector. The relative amount of each derivative was measured by gas chromatography with flame ionization detection. The areas obtained for each observed peak were used to calculate the relative amounts of each type of linkage found in the sample (Table 1). The 3,6-linked residues represent branch points.

Table 1.

	LMW	MMW	HMW
Terminal Glucose	6.4	5.1	5.4
3-Glucose	87.5	87.6	84.6
3,6-Glucose	3.2	3.8	4.0
6-Glucose	1.3	2.2	3.2
4-Glucose	0.1	0.2	0.1
Other	1.5	1.1	2.7

^{1}H NMR Spectroscopy

The samples were dissolved in DMSO-d6/D2O (6:1 by volume) at 100°C for 1 h. ^{1}HNMR Spectra were recorded at the University of Minnesota Department of Chemistry NMR lab on a Varian UNITYplus-300 spectrometer at 80°C. The spectra were collected at 300 MHz with 32 scans, a relaxation delay of 1.5 seconds, a pulse of 45°, an acquisition time of 2.0 seconds, and a spectral width of 5999 Hz. Table 2 provides ^{1}H NMR chemical shifts in all three glucans used in this study as well as literature values

bioRxiv preprint doi: https://doi.org/10.1101/824995; this version posted May 25, 2020. The copyright holder for this preprint (which was not certified by peer review) is the author/funder, who has granted bioRxiv a license to display the preprint in perpetuity. It is made available under aCC-BY 4.0 International license.

[50]. These data, taken together with other characterization methods used, do confirm that the structure of the polysaccharides used in this study conforms to expected results from fungal cell wall glucans (Table 2, Supplemental Fig. 3).

Table 2.

	H-1 (1,3-glucan)	**H-2, 4, and 5 (1,3-)**	**H-3 and 6b (1,3-)**	**H-6a (1,3-)**
LMW	4.52, d, J = 7.8 Hz, 1H	3.20-3.33 m, 3H	~3.5, m, (hidden by H_2O)	3.72, d, J = 11 Hz, 1H
MMW	4.52, d, J = 8.1 Hz, 1H	3.21-3.33 m, 3H	~3.5, m, (hidden by H_2O)	3.72, d, J = 11 Hz, 1H
HMW	4.52, d, J = 7.8 Hz, 1H	3.20-3.32 m, 3H	~3.5, m, (hidden by H_2O)	3.72, d, J = 11 Hz, 1H
Beta 1,3/1,6 Glucan Literature values	4.52, d, J = 8 Hz, 1H	3.25, m, 3H	3.46, m, 2H	3.7, d, J = 11 Hz, 1H

Microscopy and Image Analysis (Calcium Imaging & RICS/N&B)

Confocal images were obtained on an Olympus FV1000 laser scanning confocal microscope (Olympus, Center Valley, PA) built around an IX81 inverted microscope. A 10x objective lens (0.40 NA) or a super corrected 60X oil objective lens (1.40 NA), Plan-Apochromat objective lens was used for imaging. Samples were excited with a 20mW,

bioRxiv preprint doi: https://doi.org/10.1101/824995; this version posted May 25, 2020. The copyright holder for this preprint (which was not certified by peer review) is the author/funder, who has granted bioRxiv a license to display the preprint in perpetuity. It is made available under aCC-BY 4.0 International license.

473 nm diode laser and a 20 mW, 635 nm diode laser. These lines were reflected to the specimen by a 405/473/559/635 multi-edge main dichroic element followed by bandpass emission filters in front of 2 independent High sensitivity GaAsP PMT detectors (HSD1/2). Specifically, the emission light passed by the main dichroic was directed to our first detector (HSD1) via reflection from a SDM560 filter cube and passage through a BA490-540 nm bandpass filter. Our second detector (HSD2) received light passed by the SDM560 filter cube and routed through a BA575-675 nm bandpass filter.

Calcium Imaging

HEK-293 cells expressing Dectin-1A were plated at 40,000 cells in a 35 mm (MatTEK dishes) 24 hours prior to imaging. These cells were loaded with Fluo-4 and Cell Mask Deep Red (CMDR) at equimolar concentrations of 1 μM in 2 ml of media for one hour then washed before imaging. Cell Tracker Deep Red was used as a cell cytosolic volume control to account for cytosolic changes from cell contraction that occurs during stimulation. For Syk inhibition, plates were pre-treated with 250 nM of Syk Inhibitor (Calbiochem, #574711) for 30 min under normal growth environmental conditions. Images were taken at a resolution of 256 x 256 with a dwell time of 2 μs on a 10x objective lens (0.40 NA). A 20 mW, 473 nm diode laser operated at 4% power and CMDR was excited with a 20 mW, 635 nm diode laser operated at 4% power. Fluorescence of Fluo-4 was collected by a cooled GaAsP PMT set to 700V, gain 1X and offset of 0%. CMDR signal was collected by a cooled GaAsP PMT detector set to 700V, gain 1X and offset of 0%. 30 frames prior to stimulation were used to set the basal fluorescence of the fluo-4 dye. After stimulation with 100 μl of 10μg/ml of glucan, cells

bioRxiv preprint doi: https://doi.org/10.1101/824995; this version posted May 25, 2020. The copyright holder for this preprint (which was not certified by peer review) is the author/funder, who has granted bioRxiv a license to display the preprint in perpetuity. It is made available under aCC-BY 4.0 International license.

were imaged for 100 frames. To assess changes in intracellular calcium concentration, we measured the ratio of Fluo-4/CMDR intensity in order to correct for any variations in cytoplasmic volume within the confocal section across the field. This ratio was normalized to 1.0 based on mean pre-stimulation values (30 frames) and changes in calcium influx were measured as fold change of this normalized ratio (MFI fold change). For MMW denaturation experiments, soluble β-glucans were weighed and resuspended in reverse osmosis purified H_2O. In order to denature medium molecular weight glucan, we incubated MMW in DMSO or 1M NaOH. To renature the glucan from DMSO, we placed denatured MMW into Slide-A-Lyzer Dialysis Cassettes (Thermofisher, #66203) of a molecular weight cut-off of 2,000 Da and dialyzed against reverse osmosis purified H_2O for 24 hours. To renature glucan from 1M NaOH, the solution was neutralized using 1M HCl.

Protein isolation and immunoblotting

HEK-293 cells stably expressing mEmerald-Dectin-1A were seeded at 5 x 10^5 in 6-well plates 24 hours prior to the experiment. Cells were stimulated with Low, Medium and High molecular weight β-glucan (1 mg/ml) for 5 minutes, then lysed. Cells were extracted in 1X lysis buffer (43.9 mM HEPES, pH 7.5; 131.7mM NaCl; 1.1% Triton X-100; 8.8% glycerol; 1x protease inhibitor cocktail; 1mM PMSF; 1mM EGTA). Samples were centrifuged at 12,000 x *g* for 20 min at 4°C and supernatants transferred to fresh tubes. Protein concentrations were determined by Bradford assay (Bio-Rad Protein Reagent). NuPAGE LDS sample buffer (4X) with NuPAGE Sample Reducing agent (10X) was added to samples (1X final concentration). Total proteins (typically 20-50 µg) were subjected to 4-12% sodium dodecyl sulfate-polyacrylamide gel electrophoresis

bioRxiv preprint doi: https://doi.org/10.1101/824995; this version posted May 25, 2020. The copyright holder for this preprint (which was not certified by peer review) is the author/funder, who has granted bioRxiv a license to display the preprint in perpetuity. It is made available under aCC-BY 4.0 International license.

(SDS-PAGE). Proteins were transferred to Immobilon-FL PVDF transfer membrane (Millipore Sigma) using NuPAGE transfer buffer. Membranes were blocked with bovine serum albumin in Tris-buffered saline-Tween-20 (TBS-T; 20 mM Tris, 137 mM NaCl, 0.1% Tween-20) and incubated with primary antibodies overnight at 4°C. Antibodies purchased from Cell Signaling: Rabbit mAb for p-SYK (Tyr525/526) and β-Actin (13E5), and mouse mAb Syk (4D10) were used according to manufacturer's recommendations (1:1000). HRP-conjugated anti-mouse and anti-rabbit secondary antibodies (Cell Signaling or GE Healthcare) were used at a 1:10,000 dilution. Blots were visualized on a Li-Cor Odyssey FC imaging system and analyzed with Image Studio.

Biolayer interferometry

Advanced Kinetics Biolayer interferometry experiments were conducted using the Personal Assay BLItz System. Anti-human IgG Fc Capture (AHC) Biosensors tips were initially loaded with Dectin-1A:FC fusion protein (Invivogen, #fc-hdec1a) at 13 ug/ml. Binding kinetics were obtained for LMW, MMW, HMW, MMW (denatured) and MMW (renatured) at 0, 10, 50, 100, and 250 nM in triplicate. A global fitting was performed on the curves obtained using the BLItz software.

Congo Red Spectroscopic Assay

A BioTek EON Multiwell Spectrophotometer was used to analyze Congo red absorbances. A solution of 8.8 μM Congo Red, 0M-1M NaOH solution (1 M, 0.75 M, 0.5 M, 0.25 M, 0.1 M, 0.075 M, 0.05 M, 0.025 M, 0.001 M, 0 M) and LMW, MMW, or HMW β-glucans at 1 mg/ml were analyzed for the denaturation experiments. For the renaturation experiments, 1 mg/ml of β-glucan was denatured at 1M solution then renatured through neutralization with HCl 24 hrs prior to readings. DMSO denaturation

bioRxiv preprint doi: https://doi.org/10.1101/824995; this version posted May 25, 2020. The copyright holder for this preprint (which was not certified by peer review) is the author/funder, who has granted bioRxiv a license to display the preprint in perpetuity. It is made available under aCC-BY 4.0 International license.

conditions involved DMSO in water at 0%, 5% and 10%. For the DMSO renaturation experiments, DMSO was removed by dialysis (see above) prior to spectrophotometer readings. Absorbance readings were taken at 400-700 nm with 1 nm steps. All experiments were conducted in technical triplication across three independent experimental replicates.

Fluorescence Lifetime Imaging Microscopy and Förster Resonance Energy Transfer Measurement

HEK-293 cells were plated at 25,000 cells in a 35 mm (MatTEK dishes) 48h prior to imaging. Cells were transfected with mEmerald-Dectin1A-N-10 and mCherry-Dectin1A-N-10 24 hrs prior to imaging. FLIM-FRET images were obtained using a Leica DMi8 inverted microscope. A Leica Harmonic Compound PL apochromatic CS2 63X water objective with a correction collar (1.2 NA) was used for imaging. A tunable & pulsed White Light Laser (470 - 670 nm) was operated at 80 MHz at 3% laser power using a 488 nm notch filter to excite our sample. A scan speed of 200 lines/sec and a 256 x 256 pixel resolution (full field of view) was used for data acquisition. Two hybrid detectors collected at photons at (512-540 nm) and (650-700 nm) respectively on the counting mode setting. Temperature was kept at 37 °C using a Tokai Hit Stage Top Incubator for Live Cell Imaging. Lifetime images were collected using a Pico Harp 300 Fluorescence Lifetime Microscopy Time-Correlated Single Photon Counting (TCSPC) system. For our glucan stimulated cells, prior to stimulation 23 frames were collected. 230 frames were taken immediately after stimulated with β-glucans at a concentration of 10 µg/ml. Analysis was conducted on minute time points (1-5 minutes) by averaging ten frames from one minute intervals. For yeast contact site imaging studies, 3.5 x10^6 fixed yeast

bioRxiv preprint doi: https://doi.org/10.1101/824995; this version posted May 25, 2020. The copyright holder for this preprint (which was not certified by peer review) is the author/funder, who has granted bioRxiv a license to display the preprint in perpetuity. It is made available under aCC-BY 4.0 International license.

cells were resuspended in 1 ml of PBS. 100 µl of the solution was added to HEK-293 cells in 35 mm dishes 15 minutes prior to imaging. 23 frames were collected per cell. Images were collected at a maximum of 45 minutes after the addition of yeast per plate. Analysis was conducted on the plasma membrane by masking out internal cellular compartments on the images. For our fungal contact site studies, analysis was conducted on the plasma membrane that was in contact with the fungus and a separate masking for plasma membrane that was not in contact with any yeast. A bi-exponential fit was performed to the decay curve. For donor only as well as donor and acceptor on opposite sides of the plasma membrane (negative control), the decay curve indicated a negative amplitude for one of the components, thus indicating a mono-exponential decay. Therefore, decay curves from these samples were analyzed using a mono-exponential fit. For cells with donor-acceptor on the cytosolic tail, data was fit to a bi-exponential decay with the first lifetime component being locked at the donor only lifetime of 2.4 ns (τD). Lifetime values of the second component (τDA) of the decay curve were used to calculate FRET efficiency using the equation: $FRETEfficiency = \left(1 - \frac{\tau DA}{\tau D}\right) \times 100$. To determine the fraction of receptors undergoing a FRET process (Donor-Acceptor Population), the amplitude ratio between the first component (AmpD) and the second component (AmpDA) from the bi-exponential decay curve fit was calculated according to the following formula: $Donor - AcceptorPopulation = \frac{AmpDA}{(AmpD+AmpDA)} \times 100.$

Raster Image Correlation Analysis/Number and Brightness

Protocols on RICS and N&B analysis have been previously described in more depth and analysis of diffusion coefficient and receptor density were performed using SimFCS

bioRxiv preprint doi: https://doi.org/10.1101/824995; this version posted May 25, 2020. The copyright holder for this preprint (which was not certified by peer review) is the author/funder, who has granted bioRxiv a license to display the preprint in perpetuity. It is made available under aCC-BY 4.0 International license.

939 software according to these previously published procedures [54,76]. HEK-293 cells
940 expressing Emerald-Dectin1A-C-10 were plated at 40,000 cells in a 35 mm glass
941 bottom MatTEK dishes 24h prior to imaging using equipment described in “Microscopy
942 and Image Analysis” section above. Measurements were performed at the membrane
943 facing the glass coverslip. Images were collected at 256 x 256 pixel resolution on a 60×
944 1.4 NA oil immersion objective lens with a scanning zoom of 16.4X (0.050 μm vertical
945 and horizontal center to center distance between resulting image pixels). Data was
946 collected using a GaAsP PMT detector operated in photon counting mode. The 473 nm
947 diode laser operated at 0.1% power was used in these images. The Point Spread
948 Function (PSF) radial beam waist was estimated using 192 nM EFGP in solution and
949 setting the diffusion coefficient to 90 $\mu m^2/s$. Under these conditions the beam waist was
950 determined to be 0.21 μm. Immobile features were removed using a 4-frame moving
951 average subtraction. Cells were stimulated with a final concentration of 1 μg/ml of
952 glucan. After stimulation, 200 frames were collected at a pixel dwell time of 4 μs/pixel
953 (line scan of 1.096 ms) with a pinhole size of 100 μm. All cell body pixels were used for
954 analysis of N&B data from cells.
955 Images collected were also used for our Numbers and Brightness analysis; we used
956 192 nM EGFP in solution and purified mEmerald-Dectin-1 protein to set the average
957 brightness of our monomeric protein (Supplemental Fig. 4). Furthermore, the S-factor
958 was calculated using the background image. We divided each brightness distribution by
959 monomeric, dimeric, and oligomeric sections according to previous research [77]. The
960 cursors were scaled quadratically and centered at B values of 1.3, 1.6, and 2.35 for
961 monomers, dimers, and oligomers respectively.

bioRxiv preprint doi: https://doi.org/10.1101/824995; this version posted May 25, 2020. The copyright holder for this preprint (which was not certified by peer review) is the author/funder, who has granted bioRxiv a license to display the preprint in perpetuity. It is made available under aCC-BY 4.0 International license.

962 **dSTORM**

963 HEK-293 cells, were grown on cleaned and Poly-L-Lysine (0.1 mg/ml) coated coverslips
964 (~5 x 10^4 cells/coverslip) within wells of a six-well plate at 37°C 24hrs prior to the
965 experiment. The cells were then treated with MMW glucan at 1 µg/ml for 50 seconds.
966 The cells were then fixed with paraformaldehyde (PFA; 4%) for 5 minutes at 37 °C
967 followed by three washes of PBS.
968 Data acquisition was on an Olympus IX-71 microscope equipped with an objective
969 based TIRF illuminator using an oil-immersion objective (PlanApo N, 150×/1.45 NA;
970 Olympus) in an oblique illumination configuration. Sample excitation was done using a
971 637nm laser (Thorlabs, laser diode HL63133DG), with custom-built collimation optics
972 [13]. To minimize the drift that occurred during data acquisition, a self-registration
973 algorithm was implemented [78,79].
974 The Dectin-1A nanodomain density by glucan exposure engagement was quantified by
975 super resolution imaging and analyzed using H-SET as a clustering algorithm in
976 MATLAB [13]. The data for 34 cells for each condition were run through the first pass of
977 H-SET to collapse multiple observations of the blinking fluorophores into single
978 estimates of the true fluorophore locations [13]. The second H-SET pass determined
979 clustering using the DBSCAN algorithm [80] which depends on the two parameters.
980 (minPts), that is, the minimum number of objects composing a multi-cluster, and the
981 maximum distance between the objects within a multi-cluster (epsilon). We optimized
982 these parameters, defining them as 3 and 27 nm, respectively, according to optimization
983 procedures previously described [64].

984 **Collisional FRET Simulation with Monomeric Dectin-1**

bioRxiv preprint doi: https://doi.org/10.1101/824995; this version posted May 25, 2020. The copyright holder for this preprint (which was not certified by peer review) is the author/funder, who has granted bioRxiv a license to display the preprint in perpetuity. It is made available under aCC-BY 4.0 International license.

For this simulation, first a number of particles were generated based on the number of fluorophore molecules on the membrane in a specific membrane area on the real cell. As the experiments have shown that the ratio of donors to acceptors is roughly 1:1, in our model 50% of the particles were donors while the rest were acceptors. The absolute number of donor and acceptor molecules was based on the experimentally determined Dectin-1A membrane density presented in Fig. 8.

The initial location of each particle in the simulation space was defined by drawing random numbers from a uniform distribution. Throughout the simulation, particle movement was modeled by using a random walk process. The distance each particle moved at each time point was determined by the diffusion coefficient that was experimentally determined and reported in Fig. 4.

The simulation space included monomer molecules as donors and acceptors. The size of this simulation space corresponded to an experimental area equivalent to 0.16 μm^2 of the cell membrane. The total duration of the simulation was equivalent to the total amount of time required to acquire data from 5 pixels of an experimental FLIM FRET observation (equivalent to 24 μs of total data acquisition time).

To simulate a TCSPC FLIM experiment, each simulation run included 2000 sequential excitation pulses, followed by a window of simulated fluorescence decay observation with a length of 12 ns (0.1ns time resolution). At the start of each pulse, 30% of the donors were selected to act as excited particles, which corresponded with fractional donor excitation observed under our FLIM experimental conditions (Supplemental Fig. 5). Note that we consider that this value represents an upper bound on % donors excited under experimental conditions due to non-linearity in response at high laser

bioRxiv preprint doi: https://doi.org/10.1101/824995; this version posted May 25, 2020. The copyright holder for this preprint (which was not certified by peer review) is the author/funder, who has granted bioRxiv a license to display the preprint in perpetuity. It is made available under aCC-BY 4.0 International license.

powers seen in Supplemental Figure 5, which may lead the maximum photon counts to be an underestimate. However, FRET modeling conducted at <30% donors excited per pulse does not violate any model assumptions nor is it mathematically expected to yield fundamentally different results than at 30% donors excited per pulse. Moreover, simulations run at 10% donors excited per pulse to confirm this expectation showed no significant difference in model output (data not shown). A lifetime value was assigned to each excited particle by generating a random number from an exponential probability density function (τ=2.4 ns; an experimentally determined value of our donor fluorophore). This lifetime value determined how long each excited donor remained excited (in the absence of any FRET process).

At each time point, after the new location of all particles were calculated (using a random walk process), each excited donor neighborhood was checked for acceptors independently. The donor's neighborhood was defined as a disk with radius of 4-10 nm. In the case where there was an acceptor present in the region of a specific excited donor, the energy of the donor was transferred to the acceptor, according to the rate determined by all donor-acceptor pairs present within the above radial distance. The FRET efficiency for a donor and a single acceptor was calculated from the following equation:

$$E = \frac{R^6_0}{R_i^6 + R^6_0}$$

where R_0 is the Förster distance, and R_i is the distance between donor and acceptor. The FRET efficiency calculation is more complicated when a donor transfers its energy to more than a single acceptor (see "FRET efficiency" below). In both cases, the donor

bioRxiv preprint doi: https://doi.org/10.1101/824995; this version posted May 25, 2020. The copyright holder for this preprint (which was not certified by peer review) is the author/funder, who has granted bioRxiv a license to display the preprint in perpetuity. It is made available under aCC-BY 4.0 International license.

has decayed substantially. For simplicity, the acceptors that received transferred energy from a donor do not get excluded from receiving energy from another nearby donor. In our models, acceptors in this condition are rare and contribute negligibly to the model outcomes. Note that two different phenomena would result in the decay of excited donors: FRET (as explained in this paragraph) and emission (where the excited donor decays to ground state according to its characteristic fluorescence lifetime). The total probability of excited state decay is the sum of probabilities from both processes.

FRET Efficiency Calculation (Model)

With the assumption that the concentration of excited donors is lower than the acceptor concentration, we can consider only one donor molecule. In addition, if the orientation factor for dipolar coupling between donor and acceptor is identical for all donor-acceptor pairs, the FRET efficiency equation is as follows, (the pairs are considered to be rotating freely [81]):

$$E = \frac{\sum_{i}^{N} (\frac{R_0}{R_i})^6}{1 + \sum_{i}^{N} (\frac{R_0}{R_i})^6}$$

The Förster distance (R_0) of the pair of donor and acceptor fluorophores used for glucan stimulation experiments also matches that used for donors and acceptors in our FLIM FRET experiments, namely R_0= 5.24 nm [82]. The FRET efficiency in this simulation calculates the combination of FRET resulting from acceptors surrounding one excited donor, which are located with the specified radial distance.

Software

bioRxiv preprint doi: https://doi.org/10.1101/824995; this version posted May 25, 2020. The copyright holder for this preprint (which was not certified by peer review) is the author/funder, who has granted bioRxiv a license to display the preprint in perpetuity. It is made available under aCC-BY 4.0 International license.

For the RICS and N&B Data presentation and analysis we used the SimFCS Program (www.lfd.uci.edu). The calcium imaging was analyzed using ImageJ. The FLIM-FRET results were analyzed using Symphotime64 software. The BioLayer interferometry analysis was done using BLItz Pro software. Statistical analysis was performed with GraphPad Prism versions 8.2 (GraphPad Software Inc.). DSTORM analysis and FLIM-FRET modeling was performed using MATLAB using our own algorithms (https://github.com/NeumannLab/FRET-Simulation).

Acknowledgements

The authors declare that they have no conflicts of interest relevant to this work. This research was supported by the University of New Mexico Center for Spatiotemporal Modeling of Cell Signaling (STMC; NIH P50GM085273, AKN) and R01AI116894 (AKN), EUA was supported by fellowships from the STMC and an NIH T32 training grant (NIH T32 AI007538) during the course of this work. We acknowledge the competent technical assistance of Ms. Zinia Pervin in relation to BLI determinations of Dectin-1A/glucan affinity. Glucans used in this study were a generous gift of Immuno Research Inc, which played no role in experimental design, data interpretation or decision to publish. We acknowledge use of the University of New Mexico Comprehensive Cancer Center fluorescence microscopy shared facility, as well as the NIH P30CA118100 support for these cores. We would like to thank the UNM Center for Advanced Research Computing, supported in part by the National Science Foundation, for providing the high performance computing resources used for FLIM-FRET modeling in this work.

References

bioRxiv preprint doi: https://doi.org/10.1101/824995; this version posted May 25, 2020. The copyright holder for this preprint (which was not certified by peer review) is the author/funder, who has granted bioRxiv a license to display the preprint in perpetuity. It is made available under aCC-BY 4.0 International license.

1073 1. Cleveland AA, Harrison LH, Farley MM, Hollick R, Stein B, Chiller TM, et al.
1074 Declining Incidence of Candidemia and the Shifting Epidemiology of Candida
1075 Resistance in Two US Metropolitan Areas, 2008–2013: Results from Population-
1076 Based Surveillance. Chowdhary A, editor. PLoS One. 2015;10: e0120452.
1077 doi:10.1371/journal.pone.0120452
1078 2. Pfaller MA, Diekema DJ. Epidemiology of invasive candidiasis: a persistent public
1079 health problem. Clin Microbiol Rev. 2007;20: 133–63. doi:10.1128/CMR.00029-06
1080 3. Cleveland AA, Farley MM, Harrison LH, Stein B, Hollick R, Lockhart SR, et al.
1081 Changes in incidence and antifungal drug resistance in candidemia: results from
1082 population-based laboratory surveillance in Atlanta and Baltimore, 2008-2011.
1083 Clin Infect Dis. 2012;55: 1352–61. doi:10.1093/cid/cis697
1084 4. Kao AS, Brandt ME, Pruitt WR, Conn LA, Perkins BA, Stephens DS, et al. The
1085 Epidemiology of Candidemia in Two United States Cities: Results of a Population-
1086 Based Active Surveillance. Clin Infect Dis. 1999;29: 1164–1170.
1087 doi:10.1086/313450
1088 5. Hajjeh RA, Sofair AN, Harrison LH, Lyon GM, Arthington-Skaggs BA, Mirza SA, et
1089 al. Incidence of bloodstream infections due to Candida species and in vitro
1090 susceptibilities of isolates collected from 1998 to 2000 in a population-based
1091 active surveillance program. J Clin Microbiol. 2004;42: 1519–27.
1092 doi:10.1128/JCM.42.4.1519-1527.2004
1093 6. Antibiotic Resistance Threats in the United States, 2013 | Antibiotic/Antimicrobial
1094 Resistance | CDC [Internet]. [cited 24 Jul 2018]. Available:
1095 https://www.cdc.gov/drugresistance/threat-report-2013/index.html

bioRxiv preprint doi: https://doi.org/10.1101/824995; this version posted May 25, 2020. The copyright holder for this preprint (which was not certified by peer review) is the author/funder, who has granted bioRxiv a license to display the preprint in perpetuity. It is made available under aCC-BY 4.0 International license.

1096 7. Chaffin WL. Candida albicans Cell Wall Proteins. Microbiol Mol Biol Rev. 2008;72:
1097 495–544. doi:10.1128/mmbr.00032-07
1098 8. Ruiz-Herrera J, Victoria Elorza M, ValentÃ-n E, Sentandreu R. Molecular
1099 organization of the cell wall of *Candida albicans* and its relation to pathogenicity.
1100 FEMS Yeast Res. 2006;6: 14–29. doi:10.1111/j.1567-1364.2005.00017.x
1101 9. Gow NAR, Hube B. Importance of the Candida albicans cell wall during
1102 commensalism and infection. Current Opinion in Microbiology. 2012. pp. 406–
1103 412. doi:10.1016/j.mib.2012.04.005
1104 10. Ballou ER, Avelar GM, Childers DS, Mackie J, Bain JM, Wagener J, et al. Lactate
1105 signalling regulates fungal β-glucan masking and immune evasion. Nat Microbiol.
1106 2016;2. doi:10.1038/nmicrobiol.2016.238
1107 11. Sherrington SL, Sorsby E, Mahtey N, Kumwenda P, Lenardon MD, Brown I, et al.
1108 Adaptation of Candida albicans to environmental pH induces cell wall remodelling
1109 and enhances innate immune recognition. PLoS Pathog. 2017;13.
1110 doi:10.1371/journal.ppat.1006403
1111 12. Hopke A, Nicke N, Hidu EE, Degani G, Popolo L, Wheeler RT. Neutrophil Attack
1112 Triggers Extracellular Trap-Dependent Candida Cell Wall Remodeling and Altered
1113 Immune Recognition. PLoS Pathog. 2016;12. doi:10.1371/journal.ppat.1005644
1114 13. Lin J, Wester MJ, Graus MS, Lidkea KA, Neumann AK. Nanoscopic cell-wall
1115 architecture of an immunogenic ligand in Candida albicans during antifungal drug
1116 treatment. Mol Biol Cell. 2016;27: 1002–1014. doi:10.1091/mbc.E15-06-0355
1117 14. Pappas HC, Sylejmani R, Graus MS, Donabedian PL, Whitten DG, Neumann AK.
1118 Antifungal Properties of Cationic Phenylene Ethynylenes and Their Impact on β-

bioRxiv preprint doi: https://doi.org/10.1101/824995; this version posted May 25, 2020. The copyright holder for this preprint (which was not certified by peer review) is the author/funder, who has granted bioRxiv a license to display the preprint in perpetuity. It is made available under aCC-BY 4.0 International license.

Glucan Exposure. Antimicrob Agents Chemother. 2016;60: 4519–29. doi:10.1128/AAC.00317-16

15. Wheeler RT, Kombe D, Agarwala SD, Fink GR. Dynamic, morphotype-specific Candida albicans β-glucan exposure during infection and drug treatment. PLoS Pathog. 2008;4. doi:10.1371/journal.ppat.1000227

16. Wheeler RT, Fink GR. A drug-sensitive genetic network masks fungi from the immune system. PLoS Pathog. 2006;2: 328–339. doi:10.1371/journal.ppat.0020035

17. Sletmoen M, Stokke BT. Higher order structure of (1,3)-β-D-glucans and its influence on their biological activities and complexation abilities. Biopolymers. 2008;89: 310–321. doi:10.1002/bip.20920

18. Young SH, Dong WJ, Jacobs RR. Observation of a partially opened triple-helix conformation in 1→3-β- glucan by fluorescence resonance energy transfer spectroscopy. J Biol Chem. 2000;275: 11874–11879. doi:10.1074/jbc.275.16.11874

19. Chuah CT, Sarko A, Deslandes Y, Marchessault RH. Triple-Helical Crystalline Structure of Curdlan and Paramylon Hydrates. Macromolecules. 1983;16: 1375–1382. doi:10.1021/ma00242a020

20. Yoshioka Y, Uehara N, Saitô H. Conformation-dependent change in antitumor activity of linear and branched (1----3)-beta-D-glucans on the basis of conformational elucidation by carbon-13 nuclear magnetic resonance spectroscopy. Chem Pharm Bull (Tokyo). 1992;40: 1221–6. doi:10.1248/cpb.40.1221

bioRxiv preprint doi: https://doi.org/10.1101/824995; this version posted May 25, 2020. The copyright holder for this preprint (which was not certified by peer review) is the author/funder, who has granted bioRxiv a license to display the preprint in perpetuity. It is made available under aCC-BY 4.0 International license.

21. Okobira T, Miyoshi K, Uezu K, Sakurai K, Shinkai S. Molecular dynamics studies of side chain effect on the β-1,3-D-glucan triple helix in aqueous solution. Biomacromolecules. 2008;9: 783–788. doi:10.1021/bm700511d

22. Chihara G, Hamuro J, Maeda Y, Arai Y, Fukuoka F. Fractionation and purification of the polysaccharides with marked antitumor activity, especially lentinan, from Lentinus edodes (Berk.) Sing. (an edible mushroom). Cancer Res. 1970;30: 2776–81. Available: http://www.ncbi.nlm.nih.gov/pubmed/5530561

23. Zhou L, Zhang Q, Zhang Y, Liu J, Cao Y. The shiitake mushroom-derived immuno-stimulant lentinan protects against murine malaria blood-stage infection by evoking adaptive immune-responses. Int Immunopharmacol. 2009;9: 455–62. doi:10.1016/j.intimp.2009.01.010

24. Brown GD, Gordon S. Fungal β-glucans and mammalian immunity. Immunity. Cell Press; 2003. pp. 311–315. doi:10.1016/S1074-7613(03)00233-4

25. Novak M, Vetvicka V.) β-Glucans, History, and the Present: Immunomodulatory Aspects and Mechanisms of Action. J Immunotoxicol. 2008;5: 47–57. doi:10.1080/15476910802019045

26. Kim HS, Hong JT, Kim Y, Han S-B. Stimulatory Effect of β-glucans on Immune Cells. Immune Netw. 2011;11: 191. doi:10.4110/in.2011.11.4.191

27. Mueller a, Raptis J, Rice PJ, Kalbfleisch JH, Stout RD, Ensley HE, et al. The influence of glucan polymer structure and solution conformation on binding to (1--->3)-beta-D-glucan receptors in a human monocyte-like cell line. Glycobiology. 2000;10: 339–346. doi:10.1093/glycob/10.4.339

28. Zhang L, Li X, Xu X, Zeng F. Correlation between antitumor activity, molecular

bioRxiv preprint doi: https://doi.org/10.1101/824995; this version posted May 25, 2020. The copyright holder for this preprint (which was not certified by peer review) is the author/funder, who has granted bioRxiv a license to display the preprint in perpetuity. It is made available under aCC-BY 4.0 International license.

1165 weight, and conformation of lentinan. Carbohydr Res. 2005;340: 1515–21.
1166 doi:10.1016/j.carres.2005.02.032
1167 29. Elder MJ, Webster SJ, Chee R, Williams DL, Hill Gaston JS, Goodall JC. β-glucan
1168 size controls dectin-1-mediated immune responses in human dendritic cells by
1169 regulating IL-1β production. Front Immunol. 2017;8.
1170 doi:10.3389/fimmu.2017.00791
1171 30. Di Luzio NR, Williams DL, McNamee RB, Edwards BF, Kitahama A. Comparative
1172 tumor-inhibitory and anti-bacterial activity of soluble and particulate glucan. Int J
1173 cancer. 1979;24: 773–9. doi:10.1002/ijc.2910240613
1174 31. Tzianabos AO. Polysaccharide immunomodulators as therapeutic agents:
1175 structural aspects and biologic function. Clin Microbiol Rev. 2000;13: 523–33.
1176 doi:10.1128/cmr.13.4.523-533.2000
1177 32. Wang Y, Zhang L, Li Y, Hou X, Zeng F. Correlation of structure to antitumor
1178 activities of five derivatives of a β-glucan from Poria cocos sclerotium. Carbohydr
1179 Res. 2004;339: 2567–2574. doi:10.1016/j.carres.2004.08.003
1180 33. Smith AJ, Graves B, Child R, Rice PJ, Ma Z, Lowman DW, et al.
1181 Immunoregulatory Activity of the Natural Product Laminarin Varies Widely as a
1182 Result of Its Physical Properties. J Immunol. 2018;200: 788–799.
1183 doi:10.4049/jimmunol.1701258
1184 34. Suzuki T, Ohno N, Saito K, Yadomae T. Activation of the complement system by
1185 (1----3)-beta-D-glucans having different degrees of branching and different
1186 ultrastructures. J Pharmacobiodyn. 1992;15: 277–85. Available:
1187 http://www.ncbi.nlm.nih.gov/pubmed/1432567

bioRxiv preprint doi: https://doi.org/10.1101/824995; this version posted May 25, 2020. The copyright holder for this preprint (which was not certified by peer review) is the author/funder, who has granted bioRxiv a license to display the preprint in perpetuity. It is made available under aCC-BY 4.0 International license.

1188 35. Maeda YY, Watanabe ST, Chihara C, Rokutanda M. Denaturation and
1189 renaturation of a beta-1,6;1,3-glucan, lentinan, associated with expression of T-
1190 cell-mediated responses. Cancer Res. 1988;48: 671–5. Available:
1191 http://www.ncbi.nlm.nih.gov/pubmed/2446749
1192 36. Yanaki T, Ito W, Tabata K, Kojima T, Norisuye T, Takano N, et al. Correlation
1193 between the antitumor activity of a polysaccharide schizophyllan and its triple-
1194 helical conformation in dilute aqueous solution. Biophys Chem. 1983;17: 337–
1195 342. doi:10.1016/0301-4622(83)80018-0
1196 37. Duggan S, Leonhardt I, Hünniger K, Kurzai O. Host response to *Candida albicans*
1197 bloodstream infection and sepsis. Virulence. 2015; 1–11.
1198 doi:10.4161/21505594.2014.988096
1199 38. Davis SE, Hopke A, Minkin SC, Montedonico AE, Wheeler RT, Reynolds TB, et
1200 al. Masking of β(1-3)-glucan in the cell wall of Candida albicans from detection by
1201 innate immune cells depends on phosphatidylserine. Infect Immun. 2014;82:
1202 4405–13. doi:10.1128/IAI.01612-14
1203 39. Gow NAR, Netea MG, Munro CA, Ferwerda G, Bates S, Mora-Montes HM, et al.
1204 Immune recognition of Candida albicans beta-glucan by dectin-1. J Infect Dis.
1205 2007;196: 1565–71. doi:10.1086/523110
1206 40. Brown GD, Taylor PR, Reid DM, Willment JA, Williams DL, Martinez-Pomares L,
1207 et al. Dectin-1 is a major β-glucan receptor on macrophages. J Exp Med.
1208 2002;196: 407–412. doi:10.1084/jem.20020470
1209 41. Rice PJ, Adams EL, Ozment-Skelton T, Gonzalez AJ, Goldman MP, Lockhart BE,
1210 et al. Oral delivery and gastrointestinal absorption of soluble glucans stimulate

bioRxiv preprint doi: https://doi.org/10.1101/824995; this version posted May 25, 2020. The copyright holder for this preprint (which was not certified by peer review) is the author/funder, who has granted bioRxiv a license to display the preprint in perpetuity. It is made available under aCC-BY 4.0 International license.

increased resistance to infectious challenge. J Pharmacol Exp Ther. 2005;314: 1079–86. doi:10.1124/jpet.105.085415

42. O'Neill SK, Getahun A, Gauld SB, Merrell KT, Tamir I, Smith MJ, et al. Monophosphorylation of CD79a and CD79b ITAM motifs initiates a SHIP-1 phosphatase-mediated inhibitory signaling cascade required for B cell anergy. Immunity. 2011;35: 746–756. doi:10.1016/j.immuni.2011.10.011

43. Tomohiro Kurosaki B, AJohnson S, Pao L, Sada K, HirohelYamamura Ⅱ, Cambier JC. Role of the Syk Autophosphorylation Site and SH2 Domains in B Cell Antigen Receptor Signaling. doi:10.1084/jem.182.6.1815

44. Hughes CE, Pollitt AY, Mori J, Eble JA, Tomlinson MG, Hartwig JH, et al. CLEC-2 activates Syk through dimerization. Blood. 2010;115: 2947–55. doi:10.1182/blood-2009-08-237834

45. Bartel Y, Bauer B, Steinle A. Modulation of NK cell function by genetically coupled C-type lectin-like receptor/ligand pairs encoded in the human natural killer gene complex. Front Immunol. 2013;4: 362. doi:10.3389/fimmu.2013.00362

46. Hino S, Kito A, Yokoshima R, Sugino R, Oshima K, Morita T, et al. Discharge of solubilized and Dectin-1-reactive β-glucan from macrophage cells phagocytizing insoluble β-glucan particles: Involvement of reactive oxygen species (ROS)-driven degradation. Biochem Biophys Res Commun. 2012;421: 329–334. doi:10.1016/j.bbrc.2012.04.009

47. Hong F, Yan J, Baran JT, Allendorf DJ, Hansen RD, Ostroff GR, et al. Mechanism by which orally administered beta-1,3-glucans enhance the tumoricidal activity of antitumor monoclonal antibodies in murine tumor models. J Immunol. 2004;173:

bioRxiv preprint doi: https://doi.org/10.1101/824995; this version posted May 25, 2020. The copyright holder for this preprint (which was not certified by peer review) is the author/funder, who has granted bioRxiv a license to display the preprint in perpetuity. It is made available under aCC-BY 4.0 International license.

797–806. doi:10.4049/jimmunol.173.2.797

48. Gonzalez JA, Digby JD, Rice PJ, Breuel KF, DePonti WK, Kalbfleisch JH, et al. At low serum glucan concentrations there is an inverse correlation between serum glucan and serum cytokine levels in ICU patients with infections. Int Immunopharmacol. 2004;4: 1107–1115. doi:10.1016/J.INTIMP.2004.05.010

49. Digby J, Kalbfleisch J, Glenn A, Larsen A, Browder W, Williams D. Serum glucan levels are not specific for presence of fungal infections in intensive care unit patients. Clin Diagn Lab Immunol. 2003;10: 882–5. doi:10.1128/cdli.10.5.882-885.2003

50. Kim YT, Kim EH, Cheong C, Williams DL, Kim CW, Lim ST. Structural characterization of β-D-(1 → 3, 1 → 6)-linked glucans using NMR spectroscopy. Carbohydr Res. 2000;328: 331–341. doi:10.1016/S0008-6215(00)00105-1

51. Kogan G, Alföldi J, Masler L. 13C-nmr spectroscopic investigation of two yeast cell wall β-D-glucans. Biopolymers. 1988;27: 1055–1063. doi:10.1002/bip.360270702

52. Nitschke J, Modick H, Busch E, von Rekowski RW, Altenbach H-J, Mölleken H. A new colorimetric method to quantify β-1,3-1,6-glucans in comparison with total β-1,3-glucans in edible mushrooms. Food Chem. 2011;127: 791–796. doi:10.1016/J.FOODCHEM.2010.12.149

53. Brown CM, Dalal RB, Hebert B, Digman MA, Horwitz AR, Gratton E. Raster image correlation spectroscopy (RICS) for measuring fast protein dynamics and concentrations with a commercial laser scanning confocal microscope. J Microsc. 2008;229: 78–91. doi:10.1111/j.1365-2818.2007.01871.x

bioRxiv preprint doi: https://doi.org/10.1101/824995; this version posted May 25, 2020. The copyright holder for this preprint (which was not certified by peer review) is the author/funder, who has granted bioRxiv a license to display the preprint in perpetuity. It is made available under aCC-BY 4.0 International license.

1257 54. Digman MA, Stakic M, Gratton E. Raster image correlation spectroscopy and
1258 number and brightness analysis. Methods Enzymol. 2013;518: 121–44.
1259 doi:10.1016/B978-0-12-388422-0.00006-6
1260 55. Bauer B, Steinle A. HemITAM: A single tyrosine motif that packs a punch. Sci
1261 Signal. 2017;10: 1–10. doi:10.1126/scisignal.aan3676
1262 56. Brown GD. Dectin-1: a signalling non-TLR pattern-recognition receptor. Nat Rev
1263 Immunol. 2006;6: 33–43. doi:10.1038/nri1745
1264 57. Brown J, O'Callaghan CA, Marshall ASJ, Gilbert RJC, Siebold C, Gordon S, et al.
1265 Structure of the fungal beta-glucan-binding immune receptor dectin-1: implications
1266 for function. Protein Sci. 2007;16: 1042–52. doi:10.1110/ps.072791207
1267 58. Dulal HP, Adachi Y, Ohno N, Yamaguchi Y. β-Glucan-induced cooperative
1268 oligomerization of Dectin-1 C-type lectin-like domain. Glycobiology. 2018;28: 612–
1269 623. doi:10.1093/glycob/cwy039
1270 59. Singh DR, Kanvinde P, King C, Pasquale EB, Hristova K. The EphA2 receptor is
1271 activated through induction of distinct, ligand-dependent oligomeric structures.
1272 Commun Biol. 2018;1: 15. doi:10.1038/s42003-018-0017-7
1273 60. Digman MA, Dalal R, Horwitz AF, Gratton E. Mapping the number of molecules
1274 and brightness in the laser scanning microscope. Biophys J. 2008;94: 2320–32.
1275 doi:10.1529/biophysj.107.114645
1276 61. Unruh JR, Gratton E. Analysis of molecular concentration and brightness from
1277 fluorescence fluctuation data with an electron multiplied CCD camera. Biophys J.
1278 2008;95: 5385–98. doi:10.1529/biophysj.108.130310
1279 62. Trullo A, Corti V, Arza E, Caiolfa VR, Zamai M. Application limits and data

bioRxiv preprint doi: https://doi.org/10.1101/824995; this version posted May 25, 2020. The copyright holder for this preprint (which was not certified by peer review) is the author/funder, who has granted bioRxiv a license to display the preprint in perpetuity. It is made available under aCC-BY 4.0 International license.

correction in number of molecules and brightness analysis. Microsc Res Tech. 2013;76: 1135–1146. doi:10.1002/jemt.22277

63. Wester MJ, Lin J, Neumann AK. A computational model for regulation of nanoscale glucan exposure in Candida albicans. PLoS One. 2017;12. doi:10.1371/journal.pone.0188599

64. Graus MS, Wester MJ, Lowman DW, Williams DL, Kruppa MD, Martinez CM, et al. Mannan Molecular Substructures Control Nanoscale Glucan Exposure in Candida. Cell Rep. 2018;24: 2432-2442.e5. doi:10.1016/j.celrep.2018.07.088

65. Okazaki M, Adachi Y, Ohno N, Yadomae T. Structure-Activity Relationship of (1.RAR.3)-.BETA.-D-Glucans in the Induction of Cytokine Production from Macrophages, in Vitro. Biol Pharm Bull. 1995;18: 1320–1327. doi:10.1248/bpb.18.1320

66. Cleary JA, Kelly GE, Husband AJ. The effect of molecular weight and β-1,6-linkages on priming of macrophage function in mice by (1,3)-β- d -glucan. Immunol Cell Biol. 1999;77: 395–403. doi:10.1046/j.1440-1711.1999.00848.x

67. Itano MS, Graus MS, Pehlke C, Wester MJ, Liu P, Lidke KA, et al. Super-resolution imaging of C-type lectin spatial rearrangement within the dendritic cell plasma membrane at fungal microbe contact sites. Front Phys. 2014;2. doi:10.3389/fphy.2014.00046

68. Feinberg H, Guo Y, Mitchell DA, Drickamer K, Weis WI. Extended neck regions stabilize tetramers of the receptors DC-SIGN and DC-SIGNR. J Biol Chem. 2005;280: 1327–35. doi:10.1074/jbc.M409925200

69. Vitale M, Falco M, Castriconi R, Parolini S, Zambello R, Semenzato G, et al.

bioRxiv preprint doi: https://doi.org/10.1101/824995; this version posted May 25, 2020. The copyright holder for this preprint (which was not certified by peer review) is the author/funder, who has granted bioRxiv a license to display the preprint in perpetuity. It is made available under aCC-BY 4.0 International license.

Identification of NKp80, a novel triggering molecule expressed by human NK cells. Eur J Immunol. 2001;31: 233–242. doi:10.1002/1521-4141(200101)31:1<233::AID-IMMU233>3.0.CO;2-4

70. Hanč P, Schulz O, Fischbach H, Martin SR, Kjær S, Reis e Sousa C. A pH- and ionic strength-dependent conformational change in the neck region regulates DNGR-1 function in dendritic cells. EMBO J. 2016;35: 2484–2497. doi:10.15252/embj.201694695

71. Schorey JS, Lawrence C. The Pattern Recognition Receptor Dectin-1: From Fungi to Mycobacteria. Curr Drug Targets. 2008;9: 123.

72. Marakalala MJ, Kerrigan AM, Brown GD. Dectin-1: A role in antifungal defense and consequences of genetic polymorphisms in humans. Mamm Genome. 2011;22: 55–65. doi:10.1007/s00335-010-9277-3

73. Goodridge HS, Reyes CN, Becker CA, Katsumoto TR, Ma J, Wolf AJ, et al. Activation of the innate immune receptor Dectin-1 upon formation of a “phagocytic synapse”. Nature. 2011;472: 471–5. doi:10.1038/nature10071

74. Graus MS, Pehlke C, Wester MJ, Davidson LB, Steinberg SL, Neumann AK. A New Tool to Quantify Receptor Recruitment to Cell Contact Sites during Host-Pathogen Interaction. Gabhann F Mac, editor. PLoS Comput Biol. 2014;10: e1003639. doi:10.1371/journal.pcbi.1003639

75. Needs PW, Selvendran RR. Avoiding oxidative degradation during sodium hydroxide/methyl iodide-mediated carbohydrate methylation in dimethyl sulfoxide. Carbohydr Res. 1993;245: 1–10. doi:10.1016/0008-6215(93)80055-J

76. Youker RT, Teng H. Measuring protein dynamics in live cells: protocols and

bioRxiv preprint doi: https://doi.org/10.1101/824995; this version posted May 25, 2020. The copyright holder for this preprint (which was not certified by peer review) is the author/funder, who has granted bioRxiv a license to display the preprint in perpetuity. It is made available under aCC-BY 4.0 International license.

practical considerations for fluorescence fluctuation microscopy. J Biomed Opt. 2014;19: 090801. doi:10.1117/1.jbo.19.9.090801

77. Planes N, Digman MA, Vanderheyden PPML, Gratton E, Caballero-George C. Number and brightness analysis to study spatio-temporal distribution of the angiotensin II AT1 and the endothelin-1 ETA receptors: Influence of ligand binding. Biochim Biophys Acta - Gen Subj. 2019;1863: 917–924. doi:10.1016/J.BBAGEN.2019.03.004

78. Smith CS, Joseph N, Rieger B, Lidke KA. Fast, single-molecule localization that achieves theoretically minimum uncertainty. Nat Methods. 2010;7: 373–375. doi:10.1038/nmeth.1449

79. Huang F, Schwartz SL, Byars JM, Lidke KA. Simultaneous multiple-emitter fitting for single molecule super-resolution imaging. Biomed Opt Express. 2011;2: 1377. doi:10.1364/boe.2.001377

80. Ester M, Ester M, Kriegel H-P, Sander J, Xu X. A density-based algorithm for discovering clusters in large spatial databases with noise. AAAI Press. 1996; 226--231. doi=10.1.1.121.9220

81. Nyitrai M, Hild G, Lukács A, Bódis E, Somogyi B. Conformational distributions and proximity relationships in the rigor complex of actin and myosin subfragment-1. J Biol Chem. 2000;275: 2404–2409. doi:10.1074/jbc.275.4.2404

82. Akrap N, Seidel T, Barisas BG. Förster distances for fluorescence resonant energy transfer between mCherry and other visible fluorescent proteins. Anal Biochem. 2010;402: 105–106. doi:10.1016/J.AB.2010.03.026

bioRxiv preprint doi: https://doi.org/10.1101/824995; this version posted May 25, 2020. The copyright holder for this preprint (which was not certified by peer review) is the author/funder, who has granted bioRxiv a license to display the preprint in perpetuity. It is made available under aCC-BY 4.0 International license.

1349

bioRxiv preprint doi: https://doi.org/10.1101/824995; this version posted May 25, 2020. The copyright holder for this preprint (which was not certified by peer review) is the author/funder, who has granted bioRxiv a license to display the preprint in perpetuity. It is made available under aCC-BY 4.0 International license.

Supplemental Materials

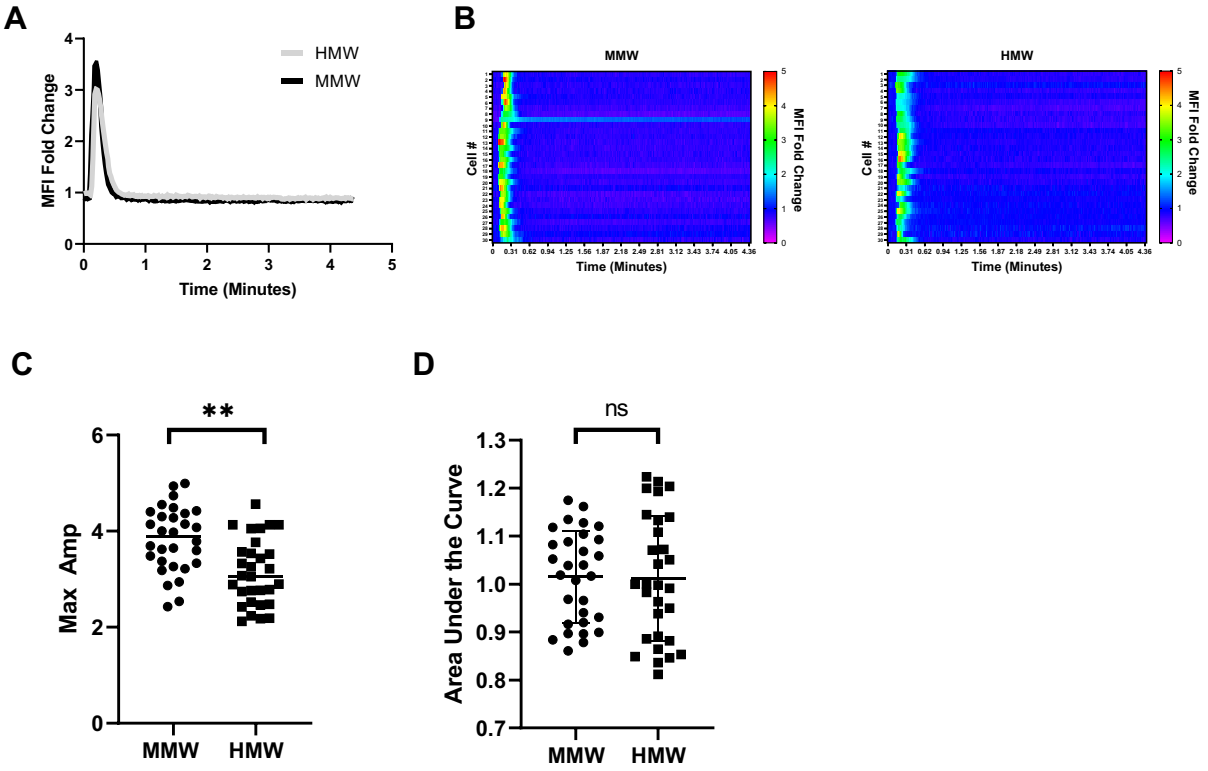

Supplemental Figure 1. Equimolar glucan stimulation of Dectin-1A exhibits similar response to MMW and HMW glucans

(A) HEK-293 cells stably transfected with Dectin-1A were loaded with Fluo-4 and Cell Tracker Deep Red at equimolar concentrations. Cell Tracker Deep Red was simultaneously loaded in order to normalize for changes in cytosolic volume caused from cell contraction. The mean fluorescence intensity of 30 cells was averaged for Dectin-1A transfected HEK-293 cells stimulated with MMW or HMW glucan at 6.67 nM. (n = 30 per glucan from 3 independent experiments per glucan). Data shown as mean fold change in volume-normalized $[Ca^{2+}]_{intracellular}$. (B) Heat maps show relative changes in intracellular calcium concentration of Dectin-1A transfected individual cells upon either addition of MMW or HMW glucan. Each row represents the normalized ratio of Fluo-4 and Cell Tracker Deep Red for a single cell over time. (C) Maximum amplitude of single cells treated with MMW or HMW glucan, as depicted in panel B. Data shown as mean ± SD (n = 30 cells); Welch's t-test, ** $p<0.001$ (D) Area under the curve of individual

bioRxiv preprint doi: https://doi.org/10.1101/824995; this version posted May 25, 2020. The copyright holder for this preprint (which was not certified by peer review) is the author/funder, who has granted bioRxiv a license to display the preprint in perpetuity. It is made available under aCC-BY 4.0 International license.

1364 traces of MMW or HMW glucan stimulated cells, as depicted in panel B. Data shown as mean ± SD (n =

1365 30 cells).

1366

bioRxiv preprint doi: https://doi.org/10.1101/824995; this version posted May 25, 2020. The copyright holder for this preprint (which was not certified by peer review) is the author/funder, who has granted bioRxiv a license to display the preprint in perpetuity. It is made available under aCC-BY 4.0 International license.

1367

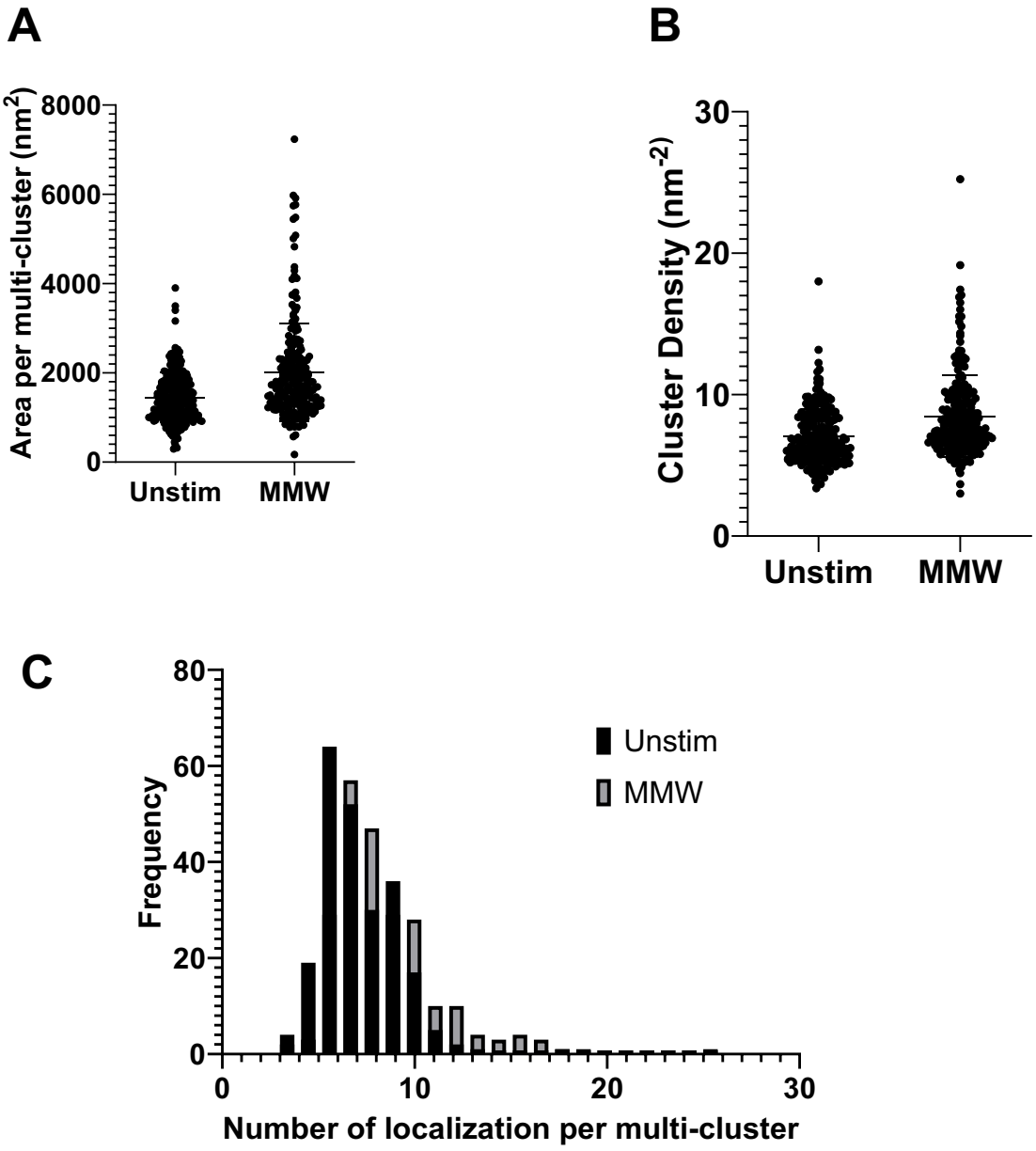

1368

1369 **Supplemental Figure 2. dSTORM clustering analysis shows similar multicluster**

1370 **characteristics in unstimulated and stimulated cells.**

1371 (A) Areas per multi-cluster in dSTORM analysis of HEK-293 cells expressing Dectin-1A unstimulated or

1372 stimulated with MMW. (B) Cluster density of dSTORM analysis of HEK-293 cells expressing Dectin-1A

bioRxiv preprint doi: https://doi.org/10.1101/824995; this version posted May 25, 2020. The copyright holder for this preprint (which was not certified by peer review) is the author/funder, who has granted bioRxiv a license to display the preprint in perpetuity. It is made available under aCC-BY 4.0 International license.

unstimulated or stimulated with MMW. (C) Histogram analysis of the number of localizations of HEK-293 cells expressing Dectin-1A unstimulated or stimulated with MMW. Data shown as mean ± SD (n = 34).

bioRxiv preprint doi: https://doi.org/10.1101/824995; this version posted May 25, 2020. The copyright holder for this preprint (which was not certified by peer review) is the author/funder, who has granted bioRxiv a license to display the preprint in perpetuity. It is made available under aCC-BY 4.0 International license.

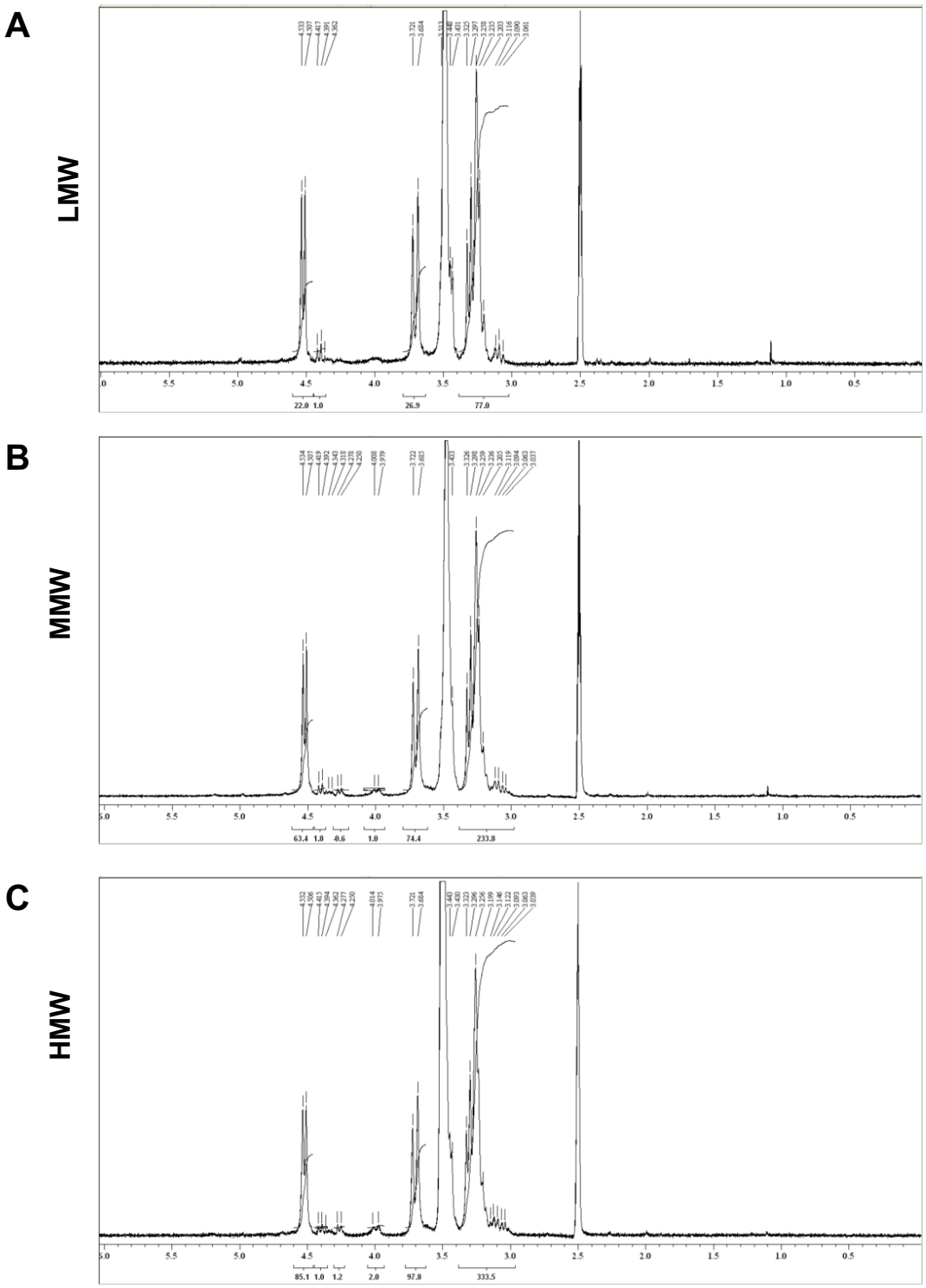

Supplemental Figure 3. ^{1}HNMR spectra of glucans used in this study.

(A) ^{1}H NMR spectrum of LMW, (B) MMW, and (C) HMW glucan.

bioRxiv preprint doi: https://doi.org/10.1101/824995; this version posted May 25, 2020. The copyright holder for this preprint (which was not certified by peer review) is the author/funder, who has granted bioRxiv a license to display the preprint in perpetuity. It is made available under aCC-BY 4.0 International license.

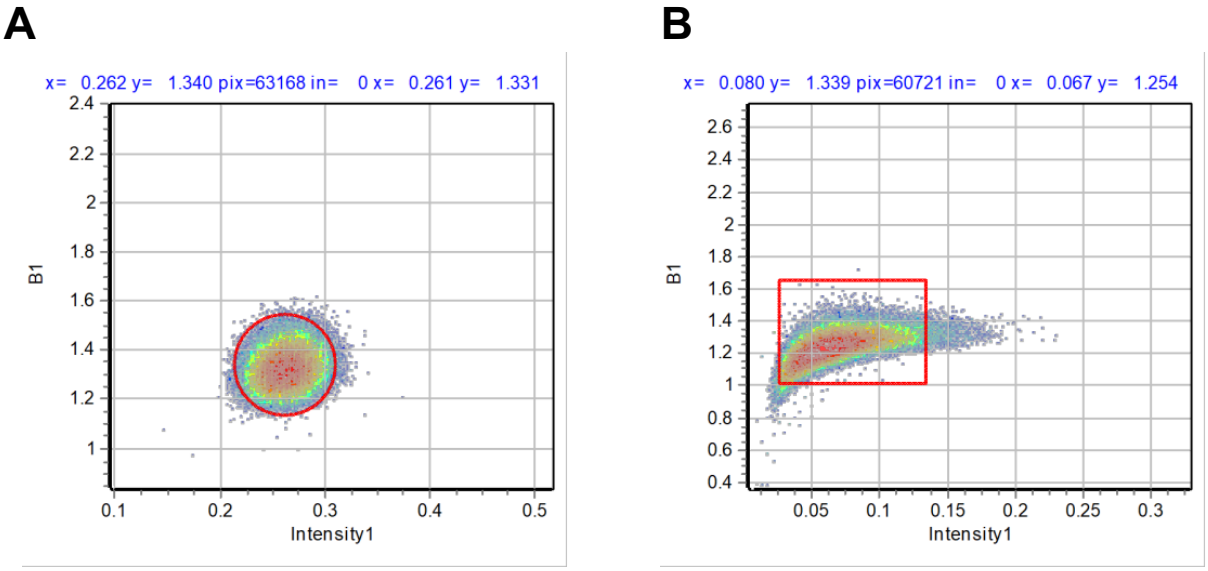

Supplemental Figure 4. Numbers and Brightness analysis calibration.

(A) Brightness vs intensity 2D histogram of purified EGFP with the selected pixels that contribute to the monomers (red circle) in the image. A brightness value of 1.34 was obtained. (B) Brightness vs intensity 2D histogram of purified mEmerald-Dectin-1A with the selected pixels that contribute to the monomers (red box) in the image. A brightness value of 1.34 was obtained.

bioRxiv preprint doi: https://doi.org/10.1101/824995; this version posted May 25, 2020. The copyright holder for this preprint (which was not certified by peer review) is the author/funder, who has granted bioRxiv a license to display the preprint in perpetuity. It is made available under aCC-BY 4.0 International license.

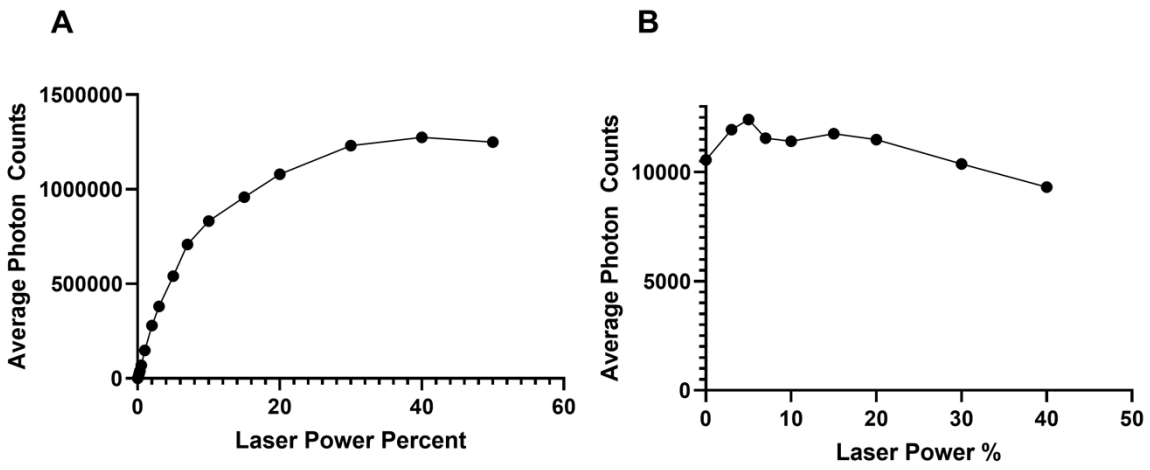

Supplemental Figure 5. Estimation of fractional donor population excited under FLIM FRET experimental conditions.

(A) Average photon counts from cells expressing mEmerald-Dectin-1A were obtained at different excitation laser powers using all other experimental conditions as described in Methods ("Fluorescence Lifetime Imaging Microscopy" section). Maximum photon counts were considered to approximate 100% donor excitation and the percent of donors excited at 3% laser power (the excitation intensity used for experiments) was obtained using the following equation:

$$\frac{PhotonCountsat3\%laserPower}{MaximumPhotonCounts} \textbf{ x 100}$$

and was used to the parameterize the FRET model. (B) To check for possible photobleaching during acquisition of data in (A), average photon counts were separately acquired (excitation at 0.1% laser power) after each laser power data point in (A) was acquired, from each individual cell. Photobleaching was negligible across the experiments conducted to obtain data in (A).

bioRxiv preprint doi: https://doi.org/10.1101/824995; this version posted May 25, 2020. The copyright holder for this preprint (which was not certified by peer review) is the author/funder, who has granted bioRxiv a license to display the preprint in perpetuity. It is made available under aCC-BY 4.0 International license.

1402 **Supplemental Table 1.**

Table of Values

	LMW	MMW	HMW
Max Calcium Amplitude	1.3 ± 0.1295	3.4 ± 0.3378	1.9 ± 0.3837

	LMW	MMW	HMW	MMW Denatured	MMW Renatured
Kd (nM)	1.93 ± 1.09	1.62 ± 0.55	0.43 ± 0.17	1.02 ± 0.37	1.22 ± 1.00

	LMW		MMW		HMW		MMW Denatured	
Min	FRET Efficiency %	Donor-Acceptor %	FRET Efficiency %	Donor-Acceptor %	FRET Efficiency %	Donor-Acceptor %	FRET Efficiency %	Donor-Acceptor %
0	83.3 ± 9.50	17.7 ± 4.97	76.5 ± 15.69	15.3 ± 7.02	86.1 ± 7.48	14.5 ± 4.66	87.5 ± 9.69	15.9 ± 5.97
1	79.1 ± 6.31	17.1 ± 6.48	77.0 ± 9.05	22.8 ± 6.54	80.1 ± 9.05	19.5 ± 5.49	86.7 ± 8.36	15.8 ± 6.06
2	79.1 ± 8.28	17.9 ± 5.98	74.3 ± 9.39	22.1 ± 8.25	78.9 ± 8.89	19.8 ± 6.20	86.2 ± 8.36	15.1 ± 6.63
3	78.5 ± 7.03	18.1 ± 5.41	77.1 ± 7.43	23.7 ± 9.13	78.9 ± 8.90	21.7 ± 6.91	86.3 ± 6.66	15.2 ± 5.68
4	78.2 ± 5.85	19.5 ± 6.89	72.1 ± 9.05	25.7 ± 8.87	79.5 ± 8.12	22.5 ± 5.40	84.1 ± 10.29	16.1 ± 5.51

bioRxiv preprint doi: https://doi.org/10.1101/824995; this version posted May 25, 2020. The copyright holder for this preprint (which was not certified by peer review) is the author/funder, who has granted bioRxiv a license to display the preprint in perpetuity. It is made available under aCC-BY 4.0 International license.

5	77.9 ± 3.96	18.8 ± 6.16	71.9 ± 7.76	28.2 ± 7.12	79.5 ± 9.14	23.7 ± 8.16	84.5 ± 11.45	14.1 ± 6.70

	N&B			RICS
	Monomers %	Dimers %	Oligomers %	Diffusion Coefficient ($\mu m^2/s$)
Unstimulated	74.0 ± 19.47	21.4 ± 18.09	4.6 ± 2.39	1.12 ± 0.50
LMW	69.5 ± 15.59	20.6 ± 9.94	9.9 ± 7.15	0.90 ± 0.46
MMW	27.5 ± 21.56	52.5 ± 15.93	20.0 ± 19.49	0.37 ± 0.24
HMW	37.5 ± 18.44	48.7 ± 14.24	13.8 ± 14.35	0.37 ± 0.18

	Singlet Cluster Density (nm^{-2})	Multiple Cluster Density (nm^{-2})	Density of Localizations (nm^{-2})	Area per cluster(nm^2)
Unstimulated	0.74 ± 0.46	0.59 ± 0.05	7.06 ± 1.95	1444 ± 559
MMW	0.77 ± 0.46	0.66 ± 0.04	8.47 ± 2.87	2016 ± 1093

	FRET Efficiency %	Donor- Acceptor %
Cell Membrane	81.8 ± 14.53	15.7 ± 8.97
SC5314	84.8 ± 8.67	15.9 ± 6.78
TRL035	78.8 ± 13.98	25.1 ± 13.06
Glucan Particle	78.8 ± 7.33	29.6 ± 13.36

1403